ACS OMEGA

http://pubs.acs.org/journal/acsodf

Article

Enhanced Adsorption and Evaluation of Tetracycline Removal in an Aquatic System by Modified Silica Nanotubes

Khalid Althumayri, Ahlem Guesmi, Wesam Abd El-Fattah, Ammar Houas, Naoufel Ben Hamadi, and Ahmed Shahat*

Cite This: *ACS Omega* 2023, 8, 6762–6777

Read Online

ACCESS | Metrics & More | Article Recommendations | Supporting Information

ABSTRACT: In the present study, a nanocomposite adsorbent based on mesoporous silica nanotubes (MSNTs) loaded with 3-aminopropyltriethoxysilane (3-APTES@MSNTs) was synthesized. The nanocomposite was employed as an effective adsorbent for the adsorption of tetracycline (TC) antibiotics from aqueous media. It has an 848.80 mg/g maximal TC adsorption capability. The structure and properties of 3-APTES@MSNT nanoadsorbent were detected by TEM, XRD, SEM, FTIR, and N_2 adsorption−desorption isotherms. The later analysis suggested that the 3-APTES@MSNT nanoadsorbent has abundant surface functional groups, effective pore size distribution, a larger pore volume, and a relatively higher surface area. Furthermore, the influence of key adsorption parameters, including ambient temperature, ionic strength, initial TC concentration, contact time, initial pH, coexisting ions, and adsorbent dosage, had also been investigated. The 3-APTES@MSNT nanoadsorbent's ability to adsorb the TC molecules was found to be more compatible with Langmuir isothermal and pseudo-second-order kinetic models. Moreover, research on temperature profiles pointed to the process' endothermic character. In combination with the characterization findings, it was logically concluded that the 3-APTES@MSNT nanoadsorbent's primary adsorption processes involved interaction, electrostatic interaction, hydrogen bonding interaction, and the pore-fling effect. The synthesized 3-APTES@MSNT nanoadsorbent has an interestingly high recyclability of >84.6 percent up to the fifth cycle. The 3-APTES@MSNT nanoadsorbent, therefore, showed promise for TC removal and environmental cleanup.

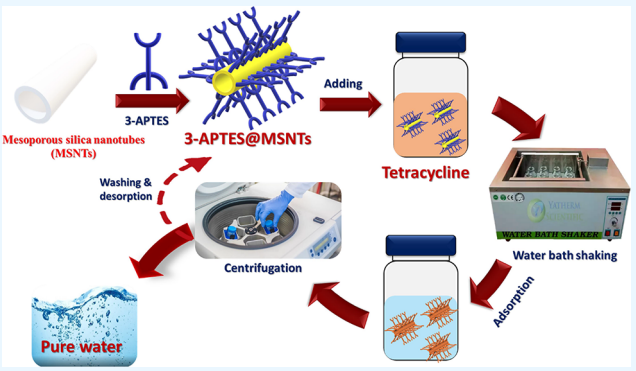

1. INTRODUCTION

Because of their potent bactericidal and antibacterial capabilities, antibiotics are often used in the medical field.[1] Tetracyclines (TCs) are among the antibiotics that are frequently used because of their effectiveness in treating bacterial infections. Although TCs are partially digested in both humans and animals, between 60 and 90 percent of TCs are excreted in their original form and parent component into the aquatic environment.[2] The widespread use of TCs and other antibiotics in the aquatic atmosphere might result in the emergence of drug-resistant bacteria, which have the potential to mutate into "superbugs" and endanger human health. The human circulatory system, liver, and hematopoietic functions can all be harmed over time by ingesting wastewater containing antibiotics, which can also make the body resistant to medication. Tetracycline removal from the environment is now a hot topic for study throughout the world in an effort to lessen the environmental and ecological risks associated with tetracycline antibiotics.[3]

To ascertain how antibiotics behave in the environment, it is critical to research their dynamics in soil. One of the primary controlling elements to stop the entry of these compounds into the food chain might be adsorption onto soil components.[4] However, this procedure is based on the properties of the antibiotics and the soil. In terms of soils, exchangeable cations, clay types, organic matter quality, and content, and pH values are important variables. In contrast, antibiotics' interactions with soils are primarily influenced by their chemical properties of functional groups, water solubility, and the number and value of their acid dissociation constants (pK_a). Additionally, it should be considered that many antibiotics might enter the soil at the same time as pollutants, which could change each antibiotic's performance with respect to interactions with soil components. There is not much research that specifically

Received: November 17, 2022
Accepted: January 24, 2023
Published: February 6, 2023

https://doi.org/10.1021/acsomega.2c07377
ACS Omega 2023, 8, 6762–6777

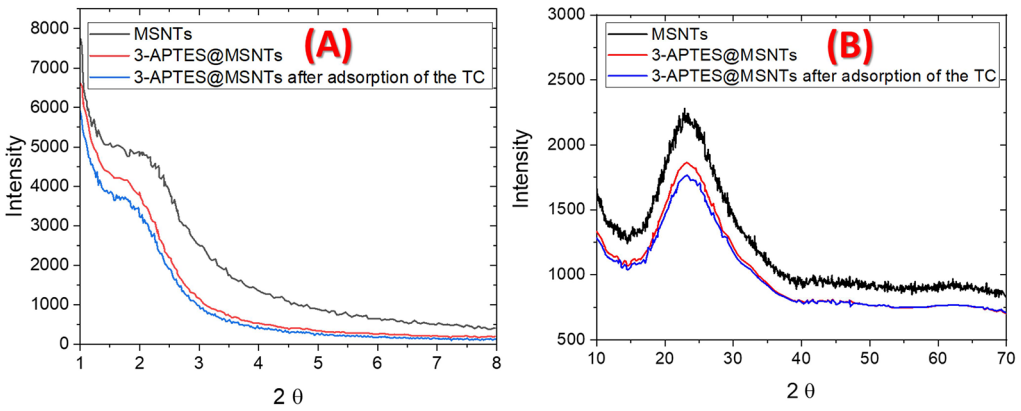

Figure 1. (A) Low-angle XRD and (B) wide-angle X-ray diffraction patterns of the MSNTs and its 3-APTES@MSNT nanoadsorbent samples before and after the adsorption of the TC molecules.

addresses the competitive adsorption of tetracyclines and sulfonamides in this context.[5]

Tetracycline has been eliminated from aqueous solutions in recent years using a variety of techniques, including adsorption-based, electrochemical, membrane, advanced oxidation, and biodegradation techniques.[6] Adsorption-based techniques offer several benefits over other techniques, including ease of design and operation, affordability, environmental safety, and great efficacy in removing small amounts of different contaminants.[7−12] To enrich low quantities of antibiotics for later breakdown, adsorption is a viable pretreatment. Mineral adsorbents, resin adsorbents, metallic oxides, and biochar materials have all been used in antibiotic adsorption. Due to their high adsorption capacity, simplicity of separation, and ease of regeneration, metallic oxides are a popular topic in the study.[13−19] The creation of defects, primarily oxygen vacancies, was a successful strategy for increasing the adsorption capacity of metallic oxide adsorbents. It has been demonstrated in several investigations that oxygen vacancies serve as capture sites and promote the adsorption of inorganic ions and TC anions.[20−26]

In order to create certain mesoporous silicas, several investigations have concentrated on the interactions between silica species and surfactants.[27−32] The interaction of the inorganic and organic components results in the spontaneous assembly of mesostructured surfactant−silica nanocomposites. The dimensions and morphologies of the resultant materials depend heavily on the kinetics of sol−gel chemistry, including the pH of the reaction solution, the amount of water present, and the reaction temperature.[13,33] This is in addition to the thermodynamics of the surfactant−silica combination.[34] The morphologies, sizes, and mesostructures of the mesoporous silicas may be tailored by carefully controlling the silica condensation rate and self-assembly.[35]

Recent interest in using mesoporous silica nanoparticles (MSNs), which have homogeneous mesopores, simple functionalization, and high biocompatibility for biomedical purposes, has increased. The huge surface area and pore chambers offer a perfect foundation for creating a multifunctional theranostic agent.[36] The different structure gives MSNs three functionally separate domains: the nanochannels/pores, the outermost surface of the nanoparticle, and the silica framework. MSNs have also been shown to have uncomplicated surface functionalization, in vivo biocompatibility, and eager cell uptake in addition to these qualities.[37−42]

We investigated the adsorption behavior, removal impact, and mechanism for functionalized mesoporous silica nanotubes for organic pollutants based on the aforementioned background. The functionalization of the mesoporous silica nanotubes was preformed by immobilization of 3-aminopropyltriethoxysilane. The prepared 3-APTES@MSNT nanoadsorbent was analyzed and characterized by transmission electron microscopy (TEM), X-ray powder diffraction (XRD), Fourier transform infrared spectroscopy (FTIR), nitrogen adsorption−desorption isotherm, and scanning electron microscopy (SEM). At the same time, the target pollutant was decided to be the antibiotic TC, and the effectiveness of the 3-APTES@MSNT nanoadsorbent for TC adsorption was investigated. Characterization investigation both before and after adsorption was coupled with kinetics and isotherm model fitting to examine the adsorption mechanism.

2. MATERIALS AND METHODS

2.1. Materials and Instruments. The Supplementary Material included detailed illustrations of all chemicals and instruments.

2.2. Synthesis of the 3-APTES@MSNT Nanoadsorbent. The MSNTs and its 3-APTES@MSNT nanoadsorbent have been synthesized previously in our previous work.[43] The synthesis process is illustrated in detail in the Supplementary Material.

2.3. Removal and Batch Studies of the 3-APTES@MSNT Nanoadsorbent. Typical batch adsorption was used to remove the tetracycline. The initial drug concentration used for the equilibrium and kinetic adsorption was 1.77×10^{-3} mol L^{-1}. The adsorbent dosage ranges from 0.01 to 0.25 g, and the temperature ranges from 293 to 323 K. With all other parameters being constant, the impact of the pH on adsorption behavior was examined in the pH range of 2−12 using either HCl or NaOH at a concentration of 0.1 mol L^{-1}. The same circumstances were used to study thermodynamic adsorption at 293, 303, and 333 K. Using a spectrophotometer with a wavelength of 446 nm, the impact of ionic strength, the TC starting concentration, adsorbent dose, and recycling was also examined.[44]

Using the global mass balance of the TC molecules in the batch eqs 1 and 2, removal percentage (percent R) and the equilibrium adsorption capacity (q_e) were computed.

https://doi.org/10.1021/acsomega.2c07377
ACS Omega 2023, 8, 6762−6777

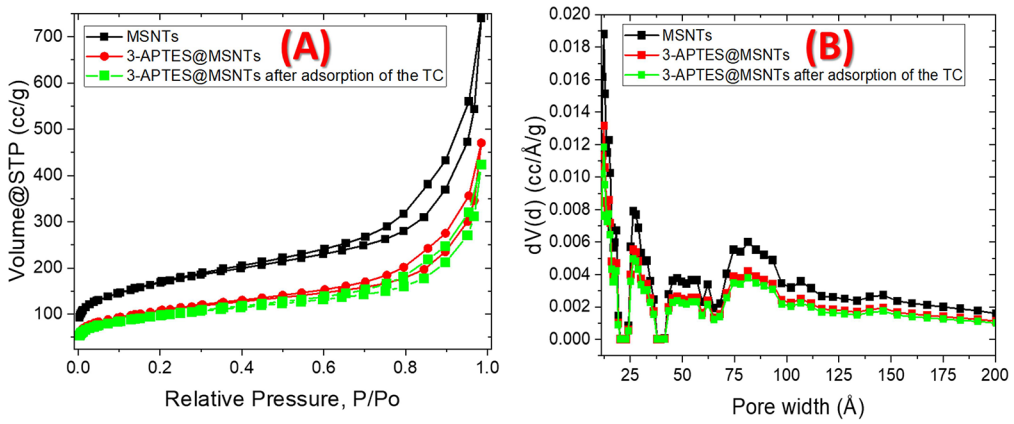

Figure 2. N_2 adsorption−desorption isotherms of the MSNTs and 3-APTES@MSNT nanoadsorbent before and after the adsorption of the TC at 77 K (A) and their pore size distribution curves (B).

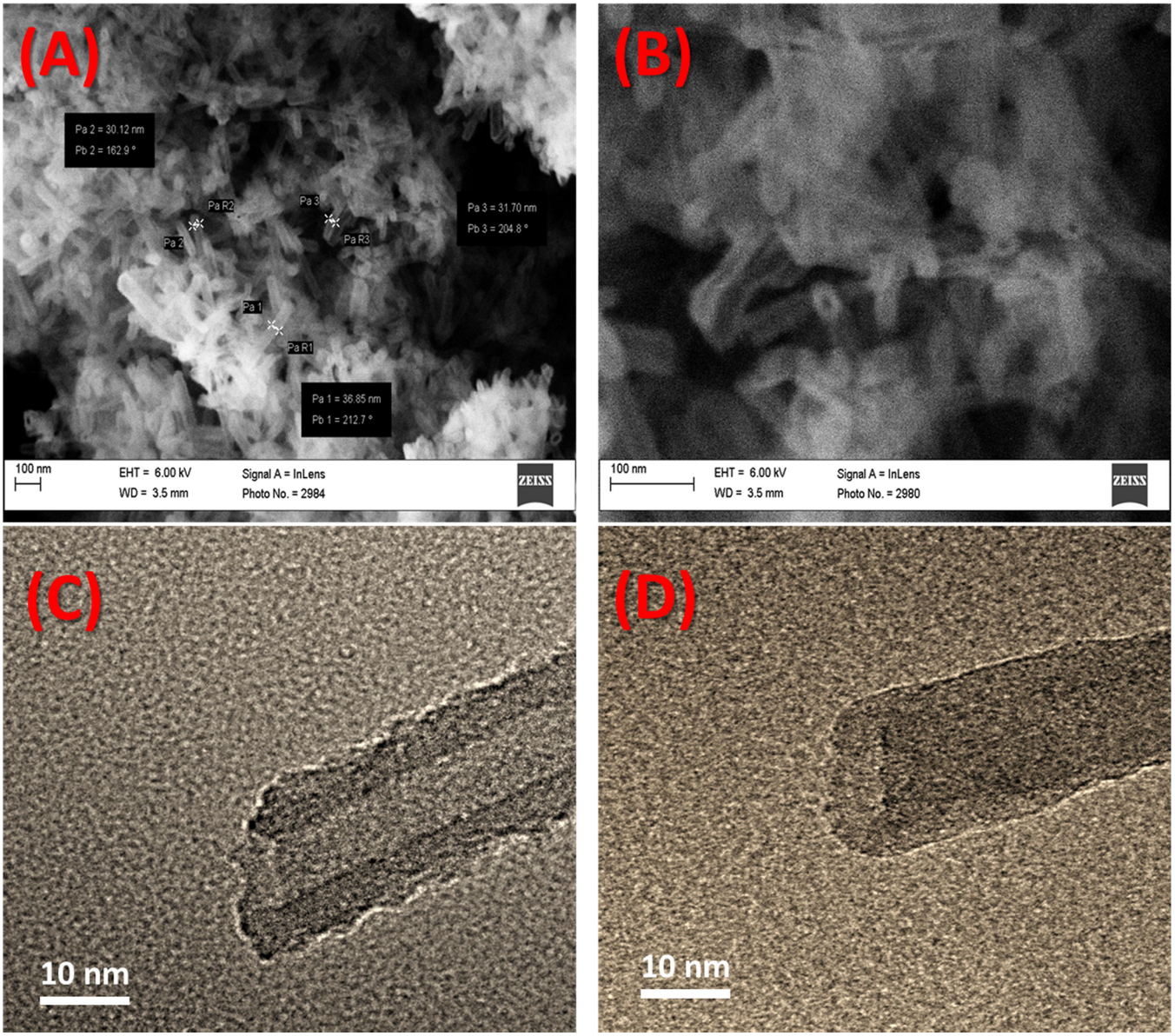

Figure 3. FE-SEM images of (A) the MSNTs and (B) the 3-APTES@MSNT nanoadsorbent and HR-TEM images of (C) the MSNTs and (D) the 3-APTES@MSNT nanoadsorbent.

https://doi.org/10.1021/acsomega.2c07377
ACS Omega 2023, 8, 6762−6777

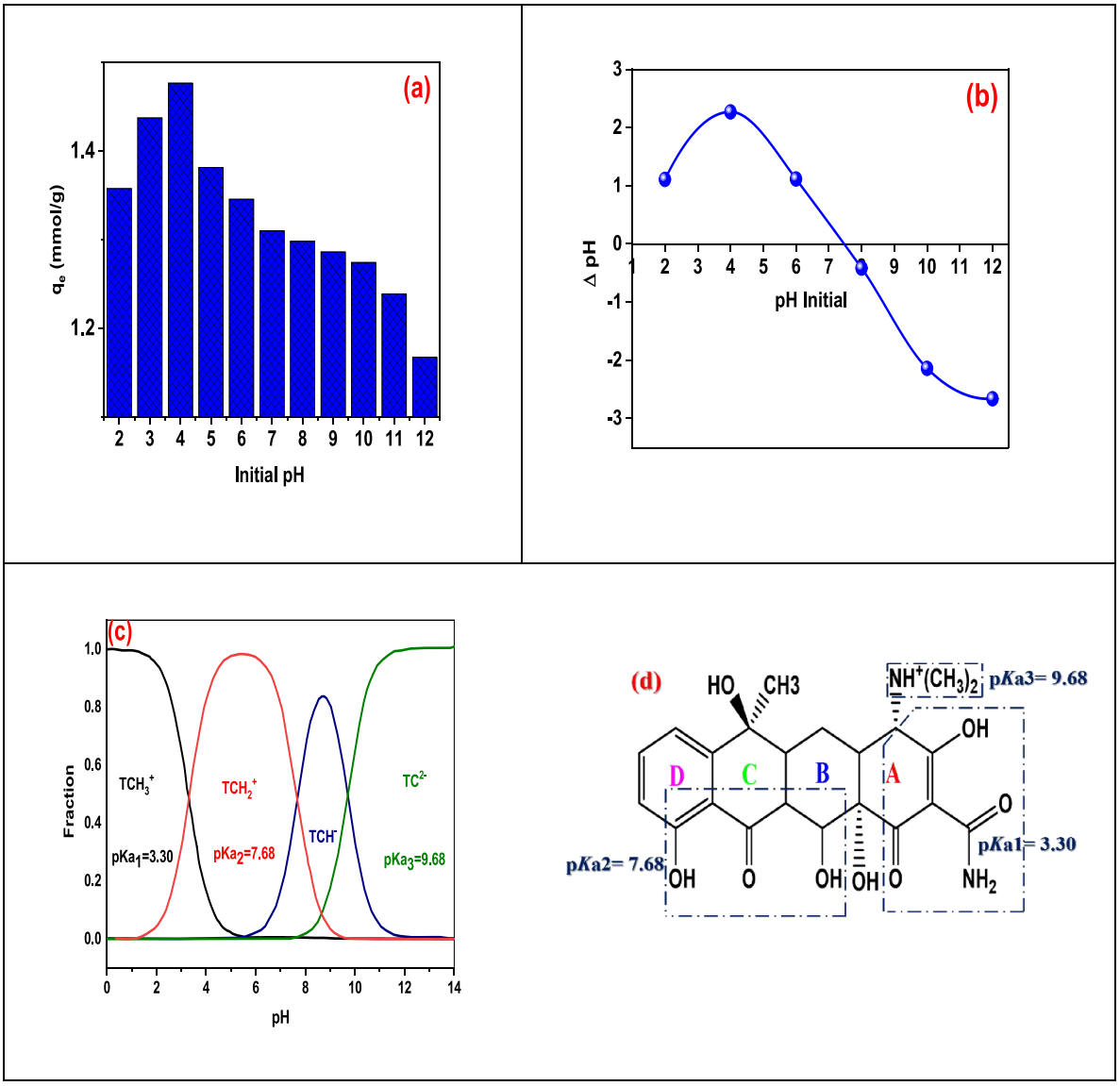

Figure 4. (a) pH of the solution's effect on the effectiveness of TC elimination. (b) pK_a of the TC. (c) pHzpc of the 3-APTES@MSNT nanoadsorbent. (d) Structural moieties associated with the three acidic dissociation constants are represented in the areas bounded by dashed lines (pK_a).

$$\%R = \frac{(C_0 - C_e)}{C_0} \times 100 \quad (1)$$

$$q_e = \frac{(C_o - C_e)V}{M} \quad (2)$$

3. RESULTS AND DISCUSSION

3.1. Characterization of the 3-APTES@MSNT Nanoadsorbent. *3.1.1. XRD Patterns.* XRD was used to confirm the 3-APTES@MSNT nanoadsorbent and MSNT structures. According to Figure 1A, the low-angle XRD patterns of them showed a peak at $2\theta \approx 1.74°$, demonstrating the existence of organized mesopores in the silica nanotubes' walls. As seen in Figure 1B, the wide angle XRD of the MSNT and 3-APTES@MSNT samples revealed a typical broad peak spanning the range 17−35°. This is explained by the discovery that the wall of the nanotubes is formed of amorphous silica. It seems that the structural morphology of the MSNTs was preserved following the alteration by 3-APTES. Moreover, the structural morphology of the 3-APTES@MSNT nanoadsorbent was investigated after the adoption process of the TC. From Figure 1A,B, results indicate that the structural morphology of the 3-APTES@MSNT nanoadsorbent did not affect the adsorption process.[45]

3.1.2. Brunauer−Emmett−Teller Specific Surface Area. The nitrogen adsorption−desorption isotherm measurements of the MSNTs and its 3-APTES@MSNT nanoadsorbent were performed. Both samples had a type IV isotherm, as seen in Figure 2A, which exhibits pore condensation and a hysteresis loop at P/P_o = 0.5−1.0 relative pressure. The (BET) surface area of the 3-APTES@MSNT nanoadsorbent was 658.34 m^2/g, which is lower than the MSNTs surface area (819.26 m^2/g). Subsequently, the MSNTs' pore volume was 0.658 cm^3/g, while the 3-APTES@MSNT nanoadsorbent pore volume was 0.532 cm^3/g. Furthermore, the pore volume and surface area of the 3-APTES@MSNT nanoadsorbent after adsorption of TC were decreased to be 0.389 cm^3/g and, 492.86 m^2/g,

https://doi.org/10.1021/acsomega.2c07377
ACS Omega 2023, 8, 6762−6777

respectively. The decline in pore volume and surface area of the 3-APTES@MSNT nanoadsorbent can be attributed to the attaching of the TC molecules inside and outside the pores on the wall of the silica nanotubes. On the other hand, the decrease in both pore volume and surface area after adsorption of the TC indicates that the removal processes may be due to pore filling.[46]

3.2. SEM and TEM Analysis. Figure 3 displays, using FE-SEM and HR-TEM, the structural morphologies of MSNTs and its 3-APTES@MSNT nanoadsorbent. They hypothesized that the material contains 33 nm-diameter nanotubes. Also, the structural morphology of the MSNTs was preserved following the alteration by 3-APTES to form the 3-APTES@MSNT nanoadsorbent.[46]

3.2.1. Fourier Transform–Infrared. The MSNTs and 3-APTES@MSNTs (FTIR) spectra were gathered and are shown in Figure S1. Both spectra contained the OH bending vibration at 787−810 cm^{-1} and the asymmetric stretching vibration of the Si−O−Si at 1066−1036 cm^{-1}. The spectra of 3-APTES@MSNTs samples revealed a new band at 2942−2930 cm^{-1} following 3-APTES was immobilized, denoting C−H stretching vibration. The NH_2 bands that showed up in 3-APTES@MSNTs at 3165 and 3239 cm^{-1} were also present.[47]

3.3. Batch Experiments. *3.3.1. Effect of pH.* Since pH has a meaningful impact on the charge of the nanoadsorbent surface (positive or negative), which is a key factor in nanoadsorbent adsorption, it is important to know what pH is best for improving the TC adsorption.[48−50] The influence of pHs in the range of 2 to 12 on the rate of the adsorption of the TC molecules by 3-APTES@MSNT nanoadsorbent was assessed in this experiment. As shown in Figure 4a, the TC's optimal absorption efficiency was at pH 4 and was 1.476 mmol/g as the pH rose from 2 to 12. Given that the pH of the experiment and the fact that the values of pK_a for the TC at various pHs along with Figure 4b are equal to 3.32, 7.68, and 9.67, the charge of the TC molecules is both negative and positive at pHs between 3.32 and 7.68. 3-APTES@MSNTs' surface charge turns positive at pHs below pHzpc because positively charged H^+ ions are present, which is shown by the observed pHzpc of 7.45. Additionally, negatively charged OH^- ions cause the surface charge of 3-APTES@MSNTs to become negative at higher pHs of pHzpc. Because there is no attraction or repulsion between the 3-APTES@MSNT nanoadsorbent and the TC molecules at pH 7.45, the adsorbent has a zero electric charge and only the physical forces that propel are responsible for the tetracycline's absorption (Figure 4c). In acidic pHs, the 3-APTES@MSNT nanoadsorbent charge is positive and the TC molecule charge is positive and negative. So, because pH affects the surface charge of the nanoadsorbent 3-APTES@MSNTs and the pK_a of the TC molecules, there is an electrostatic fascination that helps the TC molecules better adsorb on the surface. When the nanoadsorbent charge is negative and shares the same charge of the TC, a repulsive contact between the TC molecule and 3-APTES@MSNT nanoadsorbent surface is created at alkaline pHs. The rate of adsorption on the nanoadsorbent surface decreases as a result.[51]

Attenuating ionized forms of the adsorbent and adsorbate molecules can be used to explain this outcome. The pH increase affects the stacking $\pi-\pi$ bonds and the hydrogen interactions that occur during tetracycline adsorption. As a consequence, the removal dramatically decreased at higher pH. The $\pi-\pi$ and hydrogen bonds interactions between the 3-APTES@MSNT nanoadsorbent and the TC adsorbate are less advantageous under fundamental circumstances. Additionally, a drop in the removal % is justified by the anionic TCH^{1-} and TC^{2-} and OH ions' ability to impede mass transfer from the liquid phase to the surface of 3-APTES@MSNT nanoadsorbent in an alkaline media.

Tetracycline is an amphoteric chemical that mostly exists as zwitterions (Figure 4d) in the usual ambient pH range and has numerous ionizable functional groups (Figure 4c). Depending on the pH of the solution in which tetracycline is dissolved, it can go through protonation−deprotonation processes and display several ionic species. Tetracycline has reportedly had a direct impact on how it is transported, transformed, and absorbed by organisms. Thus, it is quite concerning how tetracycline gets transported throughout the environment. The adsorption of tetracycline often featured two different sorts of processes depending on the pH state, and it might display Langmuir-type or Freundlich-type isotherms.[52,53] It was also significantly impacted by pH and ionic strength. The first includes, in an acidic environment, cation exchange interactions between the surfaces of 3-APTES@MSNTs and the protonated amine group on tetracycline. The second is more beneficial to acidic and neutral circumstances and also demonstrated that it was a hydrophobic process. It includes the surface complexation of zwitterions onto the adsorbent surfaces along with proton uptake. Divalent cations increased the sorption, and under neutral or alkaline circumstances, a surface-bridging process may be in operation.[54]

3.3.2. Effect of Dose. 3-APTES@MSNT nanoadsorbent was chosen to further investigate the effect of adsorbent dose since it has demonstrated good TC adsorption ability. The increase of the dose was favorably connected with the removal efficiency of TC, although the slope gradually declined after 0.1 g. The dosage had a substantial influence on adsorption (Figure 5). More adsorption sites were produced by the greater dose, which increased the effectiveness of TC elimination. The extreme addition of adsorbent, however, cannot enhance the adsorption effect once adsorption has achieved saturation and instead results in the waste of adsorbents. The maximum adsorption capacity of the 3-APTES@MSNT nanoadsorbent was 1.4 mmol/g at a concentration of 0.02 g. The dose of 0.02 g was chosen for further investigation due to the adsorption effect and economic applicability.[55,56]

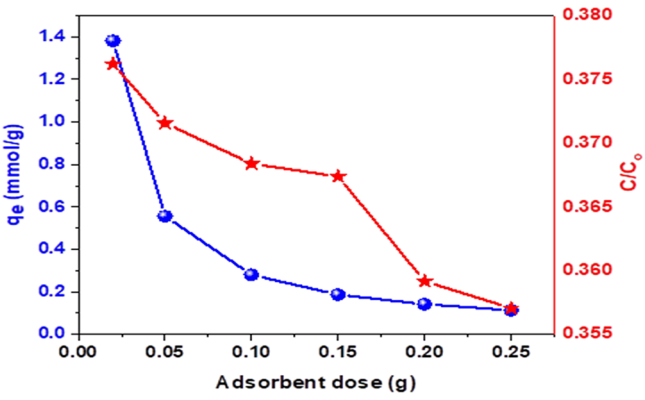

Figure 5. Sorbent dose in relation to the 3-APTES@MSNT nanoadsorbent's loading capability.

https://doi.org/10.1021/acsomega.2c07377
ACS Omega 2023, 8, 6762−6777

3.3.3. Effect of TC Concentration. TC solutions ranging in concentration from 2.76×10^{-4} to 2.2×10^{-3} mol L^{-1} at 25 °C were used to examine the effects of the TC concentration on the adsorption capacity at a constant temperature. Figure 6

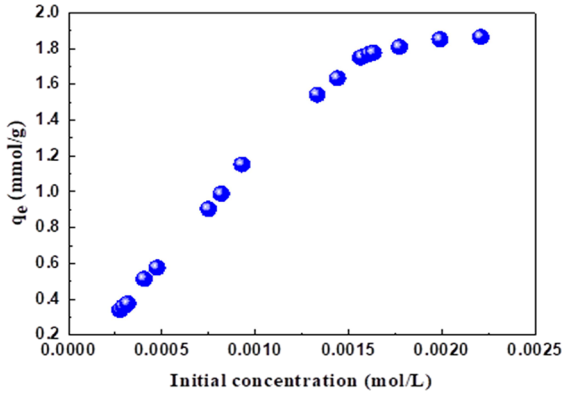

Figure 6. Effect of TC adsorption's starting concentration.

depicts the impact of the preliminary TC concentration. It implied that as the starting concentration of the adsorbate rose, so did the adsorption capability. This rise is most likely the result of vacant sites being quickly filled. Additionally, it is simple to overcome the liquid phase's mass transfer impedance to the adsorbent's surface. As the TC concentration rises, the clearance % decreases in the inverse proportion. As the lower energy sites quickly fill up during the adsorption process, the adsorbate molecules start to take up residence at the higher-energy sites, while the capacity to adsorb is directly correlated with the starting concentration. The deactivation of the adsorbent surface and the degradation of certain of the adsorption sites on the 3-APTES@MSNT nanoadsorbent surface are additional factors that contribute to a reduction in adsorption effectiveness.[57]

3.3.4. Effect of Time. Figure 7 shows the impact of contact time on the adsorption process. The clearance rate of TC was

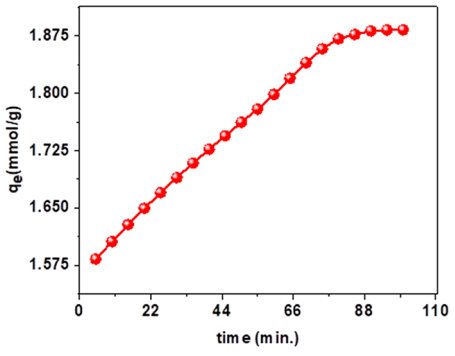

Figure 7. Effect of contact time on the TC's adsorption utilizing the nanoadsorbent 3-APTES@MSNTs.

higher in the first stages of the adsorption process because there were several adsorption sites for the TC molecule attachment on the surface of the 3-APTES@MSNT nano-adsorbent. Additionally, the adsorption rate steadily decreased as the contact time grew, and the process reached equilibrium after around 100 min. This is due to the fact that as the TC molecules adsorb to the surface of the 3-APTES@MSNT nanoadsorbent during the adsorption process, the adsorption sites were gradually occupied.

3.3.5. Effect of Temperature. Different temperatures have a substantial impact on the adsorption process, as demonstrated in Figure 8. The outcomes of the experiment revealed that the

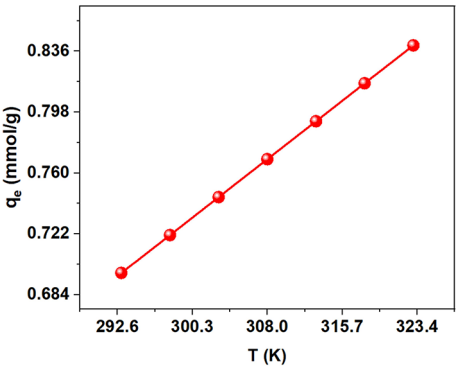

Figure 8. Effect of temperature on adsorption of the TC using the 3-APTES@MSNT nanoadsorbent.

adsorption capacity changed with temperature ($q_{e,292\ K} > q_{e,300\ K} > q_{e,308\ K} > q_{e,315\ K} > q_{e,323\ K}$). The improved adsorption impact caused by the increased temperature suggests that the 3-APTES@MSNTs' adsorption process on the TC was endothermic.

3.3.6. Adsorption Isotherm. In this regard, the loading capabilities of the 3-APTES@MSNT nanoadsorbent also rose along with the initial TC concentrations. This might be the result of an increase in loading capacity brought on by the exhaustion of the adsorptive sites on the 3-APTES@MSNT nanoadsorbent surface caused by an increase in the initial TC concentrations. The enforcement of the TC molecules from the aqueous media to 3-APTES@MSNT nanoadsorbent surface will be strongly influenced by this. The removal effectiveness decreased as the TC concentrations increased, which is the exact opposite. Four well-known isotherm models—Langmuir[58] (eq S1), Freundlich[59] (eq S2), D-R[60] (eq S3), and Temkin[61] (eq S4)—were used to investigate the phenomena occurring at the adsorbent surface throughout the adsorption process in order to conduct a more thorough assessment of the adsorption isotherm of the TC molecule using the 3-APTES@MSNT nanoadsorbent. Figure 9 depicts the linear representation of the aforementioned models, and Table S1 lists the related computed results. The examined data showed that Langmuir was more consistent with the experimental results than other isotherm models. The higher R^2 backed this up. Additionally, there should be an agreement between the theoretical and experimental loading capacities. All the aforementioned research supported the homogeneity and monolayer adsorption form of the 3-APTES@MSNT adsorbent surface. The amount of contact between the adsorbate and the surface is indicated by the Langmuir constant (K_L). The Langmuir constant, which in our instance was 68192.82 L/mol, reflects the strength of the interaction between the TC and 3-APTES@MSNT nanoadsorbent if the value of K_L is comparatively bigger. The Temkin model, which considers adsorbent saturation, believes that adsorption energy declines linearly rather than exponentially, as stated by the Freundlich pattern (Temkin constants of A and B). In concurrence, the high A and B values of 14.09 kJ/mol and 9068.06 L/mol for the TC explained the strong interaction

https://doi.org/10.1021/acsomega.2c07377
ACS Omega 2023, 8, 6762−6777

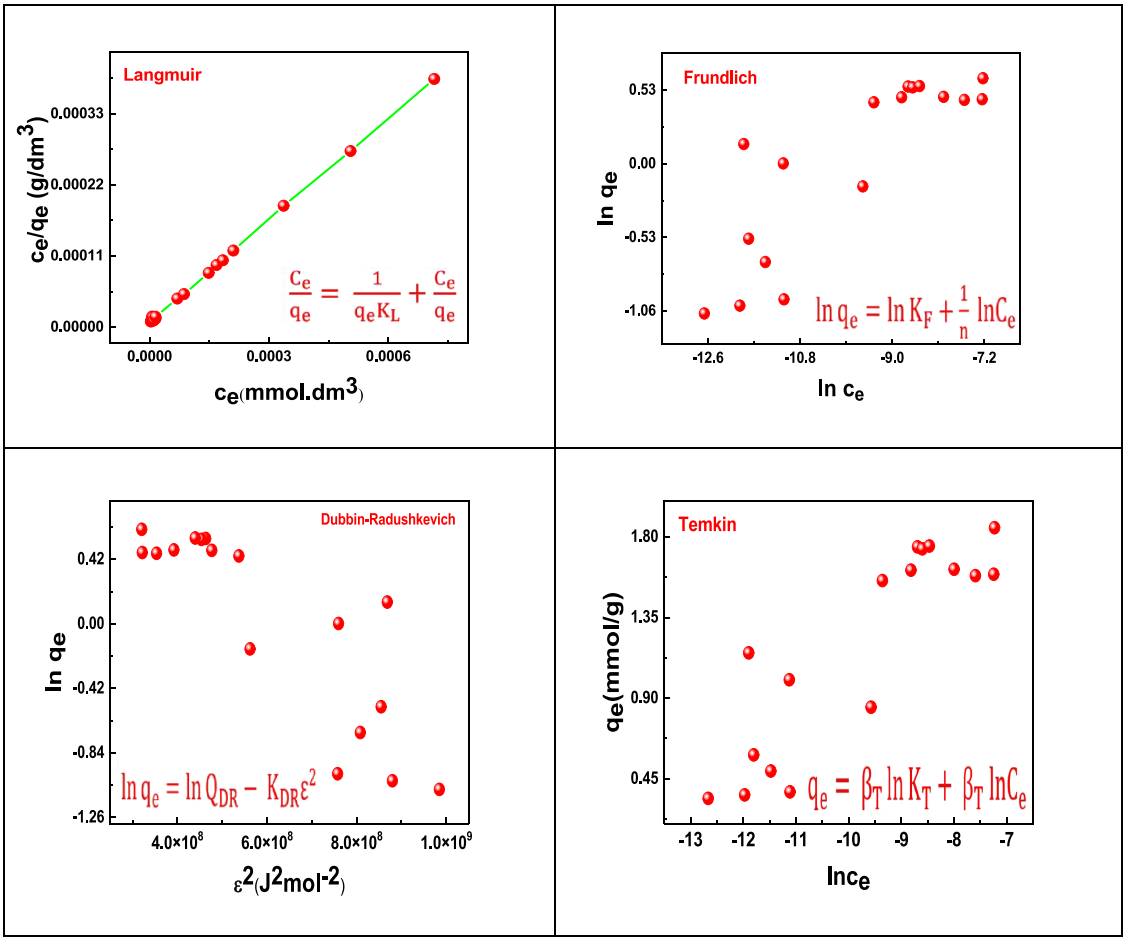

Figure 9. Adsorption isotherm models for the TC on the 3-APTES@MSNT nanoadsorbent.

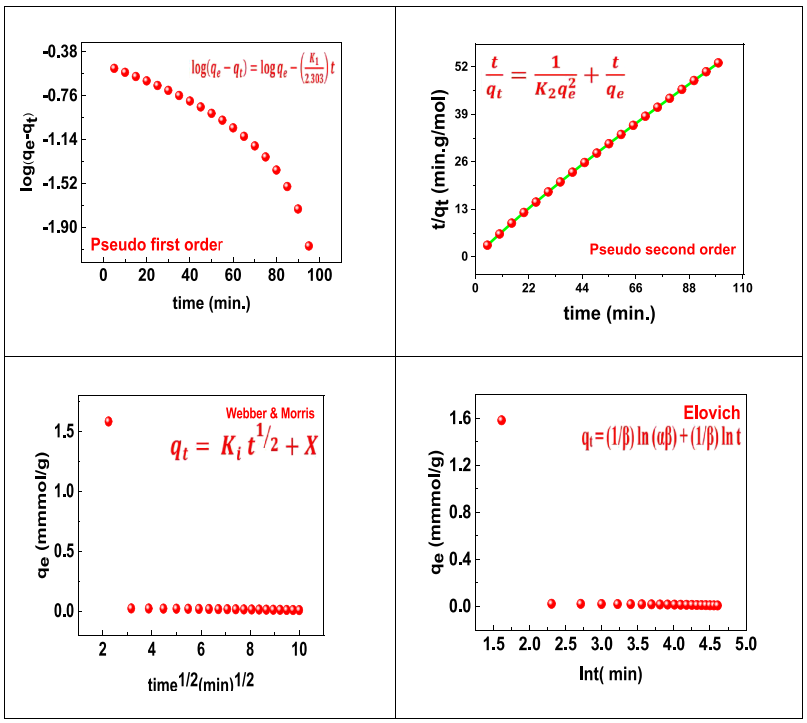

Figure 10. Adsorption kinetic models for the TC on the 3-APTES@MSNT nanoadsorbent.

https://doi.org/10.1021/acsomega.2c07377
ACS Omega 2023, 8, 6762−6777

between the TC molecules and the 3-APTES@MSNT nanoadsorbent surface. On the other hand, the binding energy that resulted from the Dubinin−Radushkevich model was 15.38 kJ/mol; this indicated that the reaction was a chemisorption process (Table S2).

3.3.7. Adsorption Kinetics. The rate of the TC adsorption on the 3-APTES@MSNT nanoadsorbent under ideal conditions was assessed using the intra-particle diffusion, Elovich, pseudo-second order, and pseudo-first-order models. There are several models used for kinetic adsorption research, but the most frequent and popular ones are pseudo-first order[62] and pseudo-second-order[63] kinetics. The pace at which adsorption processes are employed to ascertain, simulate, and carry out processes in the reaction medium has been examined through adsorption kinetics research. Equations S5 and S6 were used to compute the pseudo-second-order kinetics and pseudo-first-order kinetics. A linear relationship between the number of molecules adsorbed and the square root of the contact time shows that intra-particle diffusion is the adsorption process' level-limiting stage. Weber and Morris[64] (eq S7) created one of the most used intra-particle diffusion formulae for adsorption processes.

The level-limiting phase is more significantly impacted by surface adsorption than the steeper intercept. Since the curve could not pass through the origin when the intra-particle diffusion model was used, it was determined that intra-particle diffusion was not the main level-limiting mechanism in the kinetic research.[65]

Chemical adsorption is often applied using the Elovich equation.[66] The equation has been shown to be useful in a number of chemical adsorption processes and to cover a wide range of slow adsorption rates. Equation S8 is commonly successful in systems with diverse adsorbing surfaces.

The connection between q_t and ln t was linear, with a slope and intercept of $(1/\beta)$ and ln (β). The $1/\beta$ value reproduces the number of adsorption sites that are accessible, but the value of $(1/\beta)$ ln (β) represents the amount of adsorption when ln t is equal to zero (Figure 10).

The pseudo-second-order kinetic more closely resembles the adsorption process because the values of R^2 in Table S3 are larger than those of the pseudo-first-order kinetics. As a consequence, the pseudo-second-order kinetic model had an R^2 value of 0.998 and was the most accurate for the TC adsorption process at a concentration of 1.77×10^{-3} mol/L. They came to the conclusion that a pseudo-second-order kinetic model describes how tetracyclines adsorb (Table S3).

3.3.8. Adsorption Thermodynamics. Thermodynamic tests were performed to control the effects of temperatures of 293, 298, 303, 308, and 313 K on the TC molecule adsorption process on the 3-APTES@MSNT nanoadsorbent under optimal conditions. The three main components of entropy changes (ΔS^o), enthalpy changes (ΔH^o), and Gibbs free energy (ΔG^o) were examined in thermodynamic research. Figure 11 illustrates the thermodynamic curve for the TC adsorption.

Equations S9 and S10 were applied to compute the Gibbs free energy changes (ΔG^o), standard entropy changes (ΔS^o), and standard enthalpy changes (ΔH^o). The values of ΔS^o and ΔH^o were calculated using the slope and origin intercept of a graph of lnK_{eq} versus $1/T$ after calculating the thermodynamic equilibrium constant for the Gibbs free energy at various temperatures. Table S4's positive entropy change (ΔS^o = 75.84 J/mol K) and positive enthalpy change (ΔH^o = 19.92 kJ/mol)

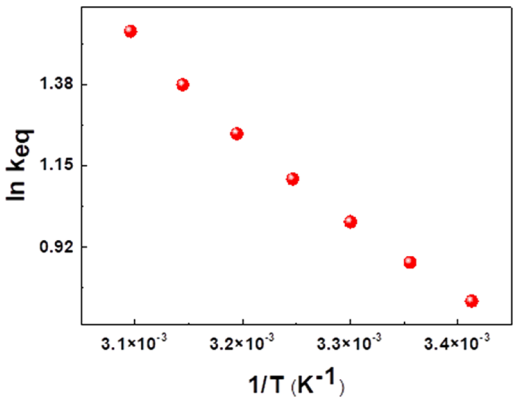

Figure 11. The inverse of temperature $(1/T)$ against lnK_{eq}.

values demonstrate that the absorption process is disrupted by the increased motility of the TC molecules in solution because the adsorption process is endothermic and the irregularity rises with temperature.[67,68]

According to the findings, it can be concluded that the 3-APTES@MSNTs nanoadsorbent's TC adsorption process is spontaneous since the quantity of Gibb's free energy negative rises with increasing temperature. It is a type of chemical adsorption because the efficiency of the adsorption process increases with temperature. Since chemical adsorption requires energy, which rises with temperature and performance, the process would operate in the opposite direction. Although both physical and chemical adsorption have always existed, chemical adsorption increases popularity as temperatures and efficiency increase, as shown in table Table S4.

3.3.9. Mechanism of Interaction. Understanding the nature of the adsorption process crucially depends on speculation about several probable processes influencing it. Generally speaking, it is controlled by the structural characteristics of both adsorbate and adsorbent. Various reactive groups, including −OH and $-NH_2$, are present on the mineral edges of the 3-APTES@MSNT nanoadsorbent, which dominate the effective binding of TC with the surface. The following factors can each be used to hypothesize a different mechanism for how they obtained adsorption onto the 3-APTES@MSNT nanoadsorbent. (i) The electrostatic attraction is frequently described as an interaction between surfaces with differing charges. It is strongly influenced by the solution's acidity and basicity as well as the carrying charge of the investigated contaminant. According to 3-APTES@MSNTs' pHpzc (7.45), protonation of exposed reactive groups under an acidic environment causes the 3-APTES@MSNTs nanoadsorbent to acquire a positive charge. Based on that, TC and positively charged particles that are present on the surface of the 3-APTES@MSNTs may interact electrostatically. (ii) Dipole−dipole interactions, or H-bonds, are produced most frequently between two hydrogen-acceptor and hydrogen-donor atoms. It often maintains the method by which different organics adsorb on MOFs. In our example, it is believed that 3-APTES@MSNTs will provide the hydrogen acceptors (from the OH groups of the silica nanotubes); however, the TC molecules will provide the hydrogen donors (i.e., oxygen-nitrogen). The quantity of hydrogen atoms in the 3-APTES@MSNT nanoadsorbent and the nitrogen/oxygen components of the investigated TC are closely correlated with the intensity of the H-bonding. These results did not support the presumption stated above, indicating that the H-bonding does not fully

https://doi.org/10.1021/acsomega.2c07377
ACS Omega 2023, 8, 6762−6777

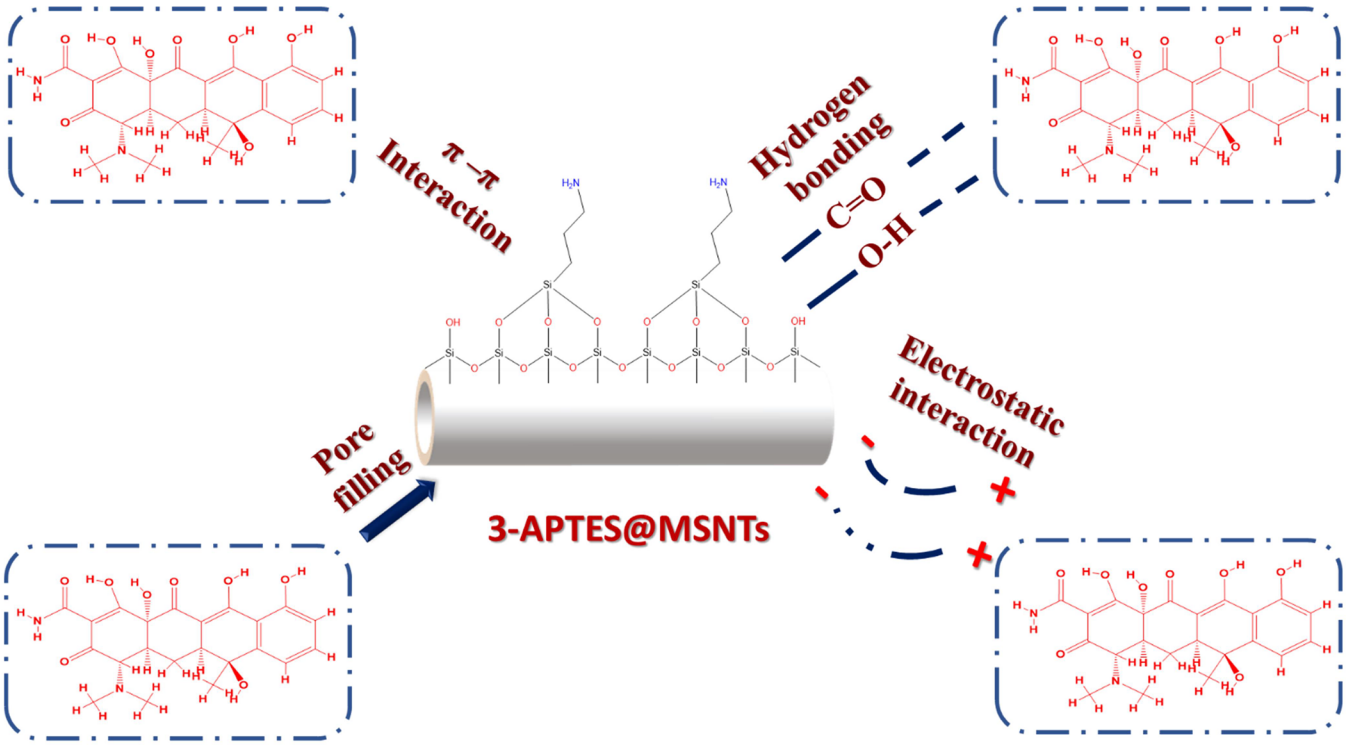

Figure 12. Mechanism of interaction between the TC and the 3-APTES@MSNT nanoadsorbent.

explain the adsorption process between the TC molecules and 3-APTES@MSNTs nanoadsorbent. (iii) As shown in Figure 12, many influential forms of contact can control the feasible adsorption process of the TC onto at 3-APTES@MSNTs nanoadsorbent.[48]

3.3.10. Effect of Salinity. Salts that have dissolved in the aqueous media are another factor that might affect the adsorption process. The ionic strength of certain contaminants can enhance the adsorbate affinity for the adsorbent and, hence, the competition for binding sites, so this parameter is crucial. In this study, several molarities of sodium chloride (0.1−1.0 mol/L) were used to explore the effect of ionic strength on TC adsorption. Figure 13 depicts the adsorption capacity of the TC molecule as a function of the presence of the ions Na^+ and Cl^-. While the adsorption capacity of the TC was 1.82 mmol/g before the addition of NaCl, it dramatically dropped (1.75 mmol/g) in the presence of a 0.01 mol/L NaCl solution. The decrease in adsorption capacity is due to the electrostatic effect of NaCl, which modifies the interaction between the TC and 3-APTES@MSNTs nanoadsorbent. Furthermore, the zwitterionic form of tetracycline is likely to interact with the ions (Na^+ and Cl^-). It is challenging for the TC molecules to bind to the functional groups of the 3-APTES@MSNT nanoadsorbent or occupy active sites due to the deprotonated group O and the protonated group NH_3^+ present in the TC molecule (competition between ions and the TC for the adsorption site). A decrease in adsorption capacity may also be explained by sodium chloride's effects on the adsorbent's specific surface area and the adsorbate's solubility.[51]

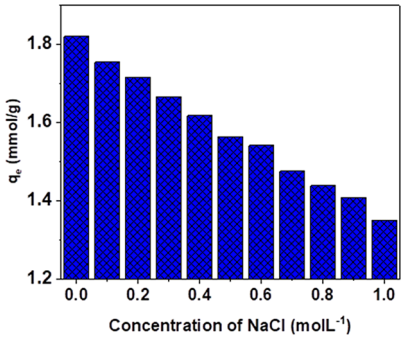

Figure 13. Effect of salinity on adsorption of the TC at the 3-APTES@MSNT nanoadsorbent.

3.3.11. Effect on Real Water Samples. In this study, the TC was removed from a genuine sample using the 3-APTES@MSNT nanoadsorbent, and the effectiveness of the TC removal was compared to the effectiveness of removing the TC molecules from a synthetic water sample. The physical and chemical characteristics of the wastewater from the actual sample, which was taken from the industrial zone water treatment lab at Suez, Egypt's wastewater treatment plant, are shown in Table 1. The sample was spiked with 8 mg/L TC, and the sample parameters were set to the ideal values on a

Table 1. Specifications of the Real Water Samples

parameter	amount
BODs	10 mg/L
TDS	1198 mg/L
TSS	86 mg/L
COD	28.6 mg/L
TC	8 mg/L
pH	8.2
sulfate	142.5 mg/L
nitrate	1.8 mg/L
phosphate	40.2 mg/L

https://doi.org/10.1021/acsomega.2c07377
ACS Omega 2023, 8, 6762−6777

synthetic sample in order to evaluate the procedure of a genuine sample. The sample was centrifuged following the procedure to remove turbidity from the actual wastewater and figure out the concentration of TC in the sample. The removal effectiveness of the TC molecules from the real sample was almost similar to 72% under ideal circumstances (temperature, 25 °C; adsorbent dose, 0.02 g/L; contact time, 30 min; TC concentration, 8 mg/L; and pH, 4), indicating good removal efficiency of TC from the real sample by this nanoadsorbent, while the clearance efficiency of the TC was greater than 95% in the synthetic sample. The results showed that the real wastewater sample had a lower TC removal efficiency than the synthetic sample. Due to the presence of ionic and soluble organic matter in the actual wastewater sample, simultaneous adsorption of competing pollutants on the 3-APTES@MSNT nanoadsorbent surface, the complexity of the wastewater matrix, and competition for the adsorption of compounds like sulfate anions, organic suspended material, and other chemical compounds, this efficiency loss can be achieved. Smaller molecules preferred to bind to the adsorbent surface groups more, occupying the active sites on the 3-APTES@MSNT nanoadsorbent surface and reducing the surface's ability to adsorb the TC molecules.[63]

3.3.12. Reusability. The study of synthetic adsorbent regeneration is crucial from an economic standpoint. A batch adsorption technique was used to assess the TC adsorption. When used under the following conditions (temperature: 25 °C, starting concentration: 5 mg/L, adsorbent dose: 0.02 g/25 mL, and pH: 4), 3-APTES@MSNT nanoadsorbent was removed by centrifuging and then regenerating with EtOH/H_2O in a 1:1 ratio. The pH of the solution was then brought up to 7 by the addition of diluted HCl or NaOH, and it was then washed many times with deionized water before being dried in an oven at 100 °C. After drying, 3-APTES@MSNT nanoadsorbent was utilized for the subsequent cycle. To assess the adsorbent's reusability, the adsorption−desorption procedure was carried out up to five times under optimal circumstances. Figure 14 demonstrates that after five cycles,

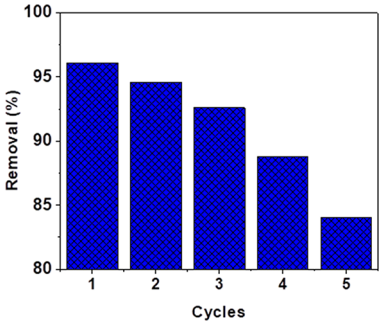

Figure 14. Reusability of the 3-APTES@MSNT nanoadsorbent during TC removal.

the removal efficacy decreased from 96.07 percent to 84.6 percent, although it was virtually maintained. After five cycles of reduction and reuse, the efficacy of TC removal may have decreased due to the irreversible occupancy of the active 3-APTES@MSNTs nanoadsorbent sites. The chemical stability of the adsorbent was assessed after the five cycles using XRD analysis.[63]

The following equation was used to get the regeneration efficiency:

$$\text{regeneration efficiency (\%)} = \frac{\text{amount of desorbed TC into the elution solution}}{\text{amount of adsorbed TC (mmol)}} \times 100 \quad (3)$$

3.3.13. Comparison with Other Adsorbents. As shown in Table S5, our adsorbent is more affordable and useful than other adsorbents and has a high removal efficiency. The results show that 3-APTES@MSNTs have a significant capacity for TC adsorption, which make it a promising adsorbent for adsorption of TC from both synthetic and natural wastewater.

4. CONCLUSIONS

In the present study, the synthesis and characterization of 3-APTES@MSNTs via SEM, BET, XRD, TEM, and FTIR proved that the adsorbent has a high pore volume and surface area of 0.532 cm^3/g and 658.34 m^2/g, respectively. The mentioned adsorbents were employed for the removal of the TC molecules from aqueous solutions. The influence of six key variables on the TC adsorption by the 3-APTES@MSNT nanoadsorbent—temperature, salinity, adsorbent dose, starting TC concentration, time, and pH—was also investigated. According to the data, at the optimum conditions (temperature: 25 °C, adsorbent dose: 0.02 g, pH: 4, and TC initial concentration: 1.77×10^{-3} mol/L), the maximum adsorption of TC was 848.80 mg/g. After five cycles of application and recovery, the 3-APTES@MSNTs nanoadsorbent still displays a removal effectiveness of around 84.6 percent. The TC adsorption process is controlled by the pseudo-second-order kinetics and Langmuir isotherm. Because this reaction is endothermic, the effectiveness of removing the TC molecules grows as the temperature rises. The 3-APTES@MSNT nanoadsorbent has rich surface functional groups, effective pore size distribution, relatively high surface area, and large pore volume. The $\pi-\pi$ interaction, H-bonding interaction, and pore-fling effect were the predominant adsorption mechanisms for the TC adsorbed on the 3-APTES@MSNT nanoadsorbent. In thermodynamic studies, the standard free energy (ΔG^o) was negative at different temperatures, suggesting the applicability and spontaneity of the process. In addition, the standard enthalpy values (ΔH^o) and standard entropy values (ΔS^o) were 19.92 kJ/mol and 7.84 J/mol, respectively, suggesting an endothermic adsorption process and a decrease in irregularity in the liquid phase. The impact of disrupting ions on the adsorption process was examined at various NaCl concentrations, and it was found using 3-APTES@MSNT nanoadsorbent that the varying concentrations of NaCl had no appreciable impact on the TC adsorption process. Because of these circumstances, antibiotic pollutants in water sources can be eliminated using the 3-APTES@MSNT nanoadsorbent. The results show that 3-APTES@MSNTs have a significant capacity for TC adsorption from both synthetic and natural wastewater.

■ ASSOCIATED CONTENT

Supporting Information

The Supporting Information is available free of charge at https://pubs.acs.org/doi/10.1021/acsomega.2c07377.

Detailed procedure for the instruments, synthesis of the MSNTs, preparation of the 3-APTES@MSNT nanoadsorbent, and the FTIR spectra of the MSNTs and its 3-APTES@MSNT nanoadsorbent (PDF)

https://doi.org/10.1021/acsomega.2c07377
ACS Omega 2023, 8, 6762−6777

AUTHOR INFORMATION

Corresponding Author

Ahmed Shahat − *Department of Chemistry, Faculty of Science, Suez University, Suez 41522, Egypt;* orcid.org/0000-0001-9198-9712; Email: ashahat@aucegypt.edu

Authors

Khalid Althumayri − *Department of Chemistry, College of Science, Taibah University, Al-Madinah Al-Munawarah 30002, Saudi Arabia*

Ahlem Guesmi − *Chemistry Department, College of Science, IMSIU (Imam Mohammad Ibn Saud Islamic University), Riyadh 11432, Saudi Arabia;* orcid.org/0000-0002-7552-4146

Wesam Abd El-Fattah − *Chemistry Department, College of Science, IMSIU (Imam Mohammad Ibn Saud Islamic University), Riyadh 11432, Saudi Arabia; Department of Chemistry, Faculty of Science, Port Said University, Port Said 42511, Egypt*

Ammar Houas − *Research Laboratory of Catalysis and Materials for Environment and Processes, University of Gabes, City Riadh Zerig, Gabes 6029, Tunisia;* orcid.org/0000-0001-8432-072X

Naoufel Ben Hamadi − *Chemistry Department, College of Science, IMSIU (Imam Mohammad Ibn Saud Islamic University), Riyadh 11432, Saudi Arabia; Faculty of Science of Monastir, Laboratory of Heterocyclic Chemistry, Natural Products and Reactivity (LR11ES39), University of Monastir, Monastir 5019, Tunisia;* orcid.org/0000-0002-2410-5275

Complete contact information is available at: https://pubs.acs.org/10.1021/acsomega.2c07377

Notes

The authors declare no competing financial interest.

ACKNOWLEDGMENTS

The authors extend their appreciation to the Deanship of Scientific Research at Imam Mohammad Ibn Saud Islamic University (IMSIU) for funding and supporting this work through Research Partnership Program no RP-21-09-70.

REFERENCES

(1) Kim, B. Y. S.; Rutka, J. T.; Chan, W. C. W. Nanomedicine. *N. Engl. J. Med.* **2010**, *363*, 2434−2443.

(2) Biju, V.; Itoh, T.; Ishikawa, M. Delivering quantum dots to cells: bioconjugated quantum dots for targeted and nonspecific extracellular and intracellular imaging. *Chem. Soc. Rev.* **2010**, *39*, 3031−3056.

(3) Gao, J.; Gu, H.; Xu, B. Multifunctional magnetic nanoparticles: design, synthesis, and biomedical applications. *Acc. Chem. Res.* **2009**, *42*, 1097−1107.

(4) Lu, A.-H.; Salabas, E. L.; Schüth, F. Magnetic nanoparticles: synthesis, protection, functionalization, and application. *Angew. Chem., Int. Ed.* **2007**, *46*, 1222−1244.

(5) Burda, C.; Chen, X.; Narayanan, R.; El-Sayed, M. A. Chemistry and properties of nanocrystals of different shapes. *Chem. Rev.* **2005**, *105*, 1025−1102.

(6) (a) Li, H.; Li, B.; Ma, J.; Ye, J.; Guo, P.; Li, L. Fate of antibiotic-resistant bacteria and antibiotic resistance genes in the electrokinetic treatment of antibiotic-polluted soil. *Chem. Eng. J.* **2018**, *337*, 584−594. (b) Liu, J.-L.; Wong, M.-H. Pharmaceuticals and personal care products (PPCPs): a review on environmental contamination in China. *Environ. Int.* **2013**, *59*, 208−224.

(7) Trewyn, B. G.; Giri, S.; Slowing, I. I.; Lin, V. S.-Y. Mesoporous silica nanoparticle based controlled release, drug delivery, and biosensor systems. *Chem. Commun.* **2007**, *31*, 3236−3245.

(8) (a) Abbas, K.; Znad, H.; Awual, M. R. A ligand anchored conjugate adsorbent for effective mercury(II) detection and removal from aqueous media. *Chem. Eng. J.* **2018**, *334*, 432−443. (b) Alam, M. M.; Uddin, M. T.; Asiri, A. M.; Fazal, M. A.; Rahman, M. M.; Islam, M. A. Fabrication of selective L-glutamic acid sensor in electrochemical technique from wet-chemically prepared RuO2 doped ZnO nanoparticles. *Mater. Chem. Phy.* **2020**, *251*, 123029. (c) Alam, M. M.; Asiri, A. M.; Uddin, M. T.; Islam, M. A.; Awual, M. R.; Rahman, M. M. One-step wet-chemical synthesis of ternary ZnO/CuO/Co3O4 nanoparticles for sensitive and selective melamine sensor development. *New J. Chem.* **2019**, *43*, 4849−4858. (d) Uddin, M. T.; Asiri, A. M.; Rahman, M. M. Detection of uric acid based on doped ZnO/Ag_2O/Co_3O_4 nanoparticle loaded glassy carbon electrode. *New J. Chem.* **2019**, *43*, 8651−8659. (e) Ali, M.; Mian, A. J.; Islam, M. N.; Awual, M. R.; Chowdhury, A. M. Physico-mechanical properties of fabrics prepared from blends of sulphonated jute fibre with natural and synthetic fibres. *Indian J. Fibre Text. Res.* **2001**, *26*, 414−417.

(9) (a) Awual, M. R. Mesoporous composite material for efficient lead(II) detection and removal from aqueous media. *J. Environ. Chem. Eng.* **2019**, *7*, 103124. (b) Awual, M. R. A facile composite material for enhanced cadmium(II) ion capturing from wastewater. *J. Environ. Chem. Eng.* **2019**, *7*, 103378. (c) Hasan, M. M. A ligand based innovative composite material for selective lead(II) capturing from wastewater. *J. Mol. Liq.* **2019**, *294*, 111679. (d) Asiri, A. M.; Rahman, M. M.; Alharthi, N. H. Assessment of enhanced nitrite removal and monitoring using ligand modified stable conjugate materials. *Chem. Eng. J.* **2019**, *363*, 64−72. (e) Islam, A.; Hasan, M. M.; Rahman, M. M.; Asiri, A. M.; Khaleque, M. A.; Sheikh, M. C. Introducing an alternate conjugated material for enhanced lead(II) capturing from wastewater. *J. Cleaner Prod.* **2019**, *224*, 920−929.

(10) (a) Hasan, M. M.; Islam, A.; Rahman, M. M.; Asiri, A. M.; Khaleque, M. A.; Sheikh, M. C. Introducing an amine functionalized novel conjugate material for toxic nitrite detection and adsorption from wastewater. *J. Cleaner Prod.* **2019**, *228*, 778−785. (b) Awual, M. R. Assessing of lead(II) capturing from contaminated wastewater using ligand doped conjugate adsorbent. *Chem. Eng. J.* **2016**, *289*, 65−73. (c) Awual, M. R. Ring size dependent crown ether based mesoporous adsorbent for high cesium adsorption from wastewater. *Chem. Eng. J.* **2016**, *303*, 539−546. (d) Hasan, M. M.; Islam, A.; Rahman, M. M.; Asiri, A. M.; Khaleque, M. A.; Sheikh, M. C. Offering an innovative composited material for effective lead(II) monitoring and removal from polluted water. *J. Cleaner Prod.* **2019**, *231*, 214−223. (e) Awual, M. R.; Khraisheh, M.; Alharthi, N. H.; Luqman, M.; Islam, A.; Karim, M. R.; Rahman, M. M.; Khaleque, M. A. Efficient detection and adsorption of cadmium(II) ions using innovative nano-composite materials. *Chem. Eng. J.* **2018**, *343*, 118−127.

(11) (a) Alharthi, N. H.; Hasan, M. M.; Karim, M. R.; Islam, A.; Znad, H.; Hossain, M. A.; Halim, M. E.; Rahman, M. M.; Khaleque, M. A. Inorganic-organic based novel nano-conjugate material for effective cobalt(II) ions capturing from wastewater. *Chem. Eng. J.* **2017**, *324*, 130−139. (b) Awual, M. R. Efficient phosphate removal from water for controlling eutrophication using novel composite adsorbent. *J. Clean. Prod.* **2019**, *228*, 1311−1319. (c) Awual, M. R. Novel ligand functionalized composite material for efficient copper-(II) capturing from wastewater sample. *Compos. B Eng.* **2019**, *172*, 387−396. (d) Hasan, M. M.; Rahman, M. M.; Asiri, A. M. Novel composite material for selective copper(II) detection and removal from aqueous media. *J. Mol. Liq.* **2019**, *283*, 772−780. (e) Hasan, M. M.; Asiri, A. M.; Rahman, M. M. Cleaning the arsenic(V) contaminated water for safe-guarding the public health using novel composite material. *Compos. B Eng.* **2019**, *171*, 294−301.

(12) (a) Awual, M. R.; Hasan, M. M.; Eldesoky, G. E.; Khaleque, M. A.; Rahman, M. M.; Naushad, M. Facile mercury detection and removal from aqueous media involving ligand impregnated conjugate nanomaterials. *Chem. Eng. J.* **2016**, *290*, 243−251. (b) Awual, M. R. Innovative composite material for efficient and highly selective Pb(II)

ion capturing from wastewater. *J. Mol. Liq.* **2019**, *284*, 502−510. (c) Awual, M. R. Novel conjugated hybrid material for efficient lead(II) capturing from contaminated wastewater. *Mater. Sci. Eng. C* **2019**, *101*, 686−695. (d) Hasan, M. M.; Khaleque, M. A.; Shiekh, M. C. Treatment of copper(II) containing wastewater by a newly developed ligand based facial conjugate materials. *Chem. Eng. J.* **2016**, *288*, 368−376. (e) Awual, M. R.; Miyazaki, M.; Taguchi, T.; Shiwaku, H.; Yaita, T. Encapsulation of cesium from contaminated water with highly selective facial organic-inorganic mesoporous hybrid adsorbent. *Chem. Eng. J.* **2016**, *291*, 128−137.

(13) Pan, Y.; Zhang, Y.; Zhou, M.; Cai, J.; Li, X.; Tian, Y. Synergistic degradation of antibiotic sulfamethazine by novel pre-magnetized Fe0/PS process enhanced by ultrasound. *Chem. Eng. J.* **2018**, *354*, 777−789.

(14) (a) Liu, S.; Mei, L.; Liang, X.; Liao, L.; Lv, G.; Ma, S.; Lu, S.; Abdelkader, A.; Xi, K. Anchoring Fe3O4 nanoparticles on carbon nanotubes for microwave-induced catalytic degradation of antibiotics. *ACS Appl. Mater. Interfaces* **2018**, *10*, 29467−29475. (b) Zeng, Z.; Ye, S.; Wu, H.; Xiao, R.; Zeng, G.; Liang, J.; Zhang, C.; Yu, J.; Fang, Y.; Song, B. Research on the sustainable efficacy of g-MoS2 decorated biochar nanocomposites for removing tetracycline hydrochloride from antibiotic-polluted aqueous solution. *Sci. Total Environ.* **2019**, *648*, 206−217.

(15) (a) Awual, M. R. A novel facial composite adsorbent for enhanced copper(II) detection and removal from wastewater. *Chem. Eng. J.* **2015**, *266*, 368−375. (b) Hasan, M. M.; Iqbal, J.; Islam, A.; Islam, M. A.; Khandaker, S.; Asiri, A. M.; Rahman, M. M. Ligand based sustainable composite material for sensitive nickel(II) capturing in aqueous media. *J. Environ. Chem. Eng.* **2020**, *8*, 103591. (c) Awual, M. R.; Hasan, M. M.; Islam, A.; Asiri, A. M.; Rahman, M. M. Optimization of an innovative composited material for effective monitoring and removal of cobalt(II) from wastewater. *J. Mol. Liq.* **2020**, *298*, 112035. (d) Awual, M. R. An efficient composite material for selective lead(II) monitoring and removal from wastewater. *J. Environ. Chem. Eng.* **2019**, *7*, 103087. (e) Hasan, M. M.; Asiri, A. M.; Rahman, M. M. Novel optical composite material for efficient vanadium(III) capturing from wastewater. *J. Mol. Liq.* **2019**, *283*, 704−712.

(16) (a) Awual, M. R. Solid phase sensitive palladium(II) ions detection and recovery using ligand based efficient conjugate nanomaterials. *Chem. Eng. J.* **2016**, *300*, 264−272. (b) Awual, M. R.; Yaita, T.; Miyazaki, Y.; Matsumura, D.; Shiwaku, H.; Taguchi, T. A reliable hybrid adsorbent for efficient radioactive cesium accumulation from contaminated wastewater. *Sci. Rep.* **2016**, *6*, 19937. (c) Hasan, M. M. Fine-tuning mesoporous adsorbent for simultaneous ultra-trace palladium(II) detection, separation and recovery. *J. Ind. Eng. Chem.* **2015**, *21*, 507−515. (d) Awual, M. R.; Hasan, M. M. Colorimetric detection and removal of copper(II) ions from wastewater samples using tailor-made composite adsorbent. *Sens. Actuators, B* **2015**, *206*, 692−700. (e) Awual, M. R.; Eldesoky, G. E.; Yaita, T.; Naushad, M.; Shiwaku, H.; AlOthman, Z. A.; Suzuki, S. Schiff based ligand containing nano-composite adsorbent for optical copper(II) ions removal from aqueous solutions. *Chem. Eng. J.* **2015**, *279*, 639−647.

(17) (a) Awual, M. R. Investigation of potential conjugate adsorbent for efficient ultra−trace gold(III) detection and recovery. *J. Ind. Eng. Chem.* **2014**, *20*, 3493−3501. (b) Ismael, M. Efficient gold(III) detection, separation and recovery from urban mining waste using a facial conjugate adsorbent. *Sens. Actuators, B* **2014**, *196*, 457−466. (c) Awual, M. R.; Hasan, M. M. Novel conjugate adsorbent for visual detection and removal of toxic lead(II) ions from water. *Microporous Mesoporous Mater.* **2014**, *196*, 261−269. (d) Yaita, T.; Okamoto, Y. A novel ligand based dual conjugate adsorbent for cobalt(II) and copper(II) ions capturing from water. *Sens. Actuatuators, B* **2014**, *203*, 71−80. (e) Awual, M. R.; Ismael, M.; Khaleque, M. A.; Yaita, T. Ultra-trace copper(II) detection and removal from wastewater using novel meso-adsorbent. *J. Ind. Eng. Chem.* **2014**, *20*, 2332−2340.

(18) (a) Arshad, M. N.; Sheikh, T. A.; Rahman, M. M.; Asiri, A. M.; Marwani, H. M.; Awual, M. R. Fabrication of cadmium ionic sensor based on (E)-4-Methyl-N′-(1-(pyridin-2-yl) ethylidene) benzenesulfonohydrazide (MPEBSH) by electrochemical approach. *J. Organomet. Chem.* **2017**, *827*, 49−55. (b) Yaita, T.; Kobayashi, T.; Shiwaku, H.; Suzuki, S. Improving cesium removal to clean-up the contaminated water using modified conjugate material. *J. Environ. Chem. Eng.* **2020**, *8*, 103684. (c) Awual, M. R.; Hasan, M. M.; Iqbal, J.; Islam, A.; Islam, M. A.; Asiri, A. M.; Rahman, M. M. Naked-eye lead(II) capturing from contaminated water using innovative large-pore facial composite materials. *Microchem. J.* **2020**, *154*, 104585. (d) Awual, M. R. New type mesoporous conjugate material for selective optical copper(II) ions monitoring & removal from polluted waters. *Chem. Eng. J.* **2017**, *307*, 85−94. (e) Alharthi, N. H.; Okamoto, Y.; Karim, M. R.; Halim, M. E.; Hasan, M. M.; Rahman, M. M.; Islam, M. M.; Khaleque, M. A.; Sheikh, M. C. Ligand field effect for Dysprosium(III) and Lutetium(III) adsorption and EXAFS coordination with novel composite nanomaterials. *Chem. Eng. J.* **2017**, *320*, 427−435.

(19) (a) Awual, M. R.; Yaita, T.; Shiwaku, H.; Suzuki, S. A sensitive ligand embedded nano-conjugate adsorbent for effective cobalt(II) ions capturing from contaminated water. *Chem. Eng. J.* **2015**, *276*, 1−10. (b) Yaita, T.; Suzuki, S.; Shiwaku, H. Ultimate selenium(IV) monitoring and removal from water using a new class of organic ligand based composite adsorbent. *J. Hazard. Mater.* **2015**, *291*, 111−119. (c) Awual, M. R. Novel nanocomposite materials for efficient and selective mercury ions capturing from wastewater. *Chem. Eng. J.* **2017**, *307*, 456−465. (d) Hasan, M. M.; Shahat, A.; Naushad, M.; Shiwaku, H.; Yaita, T. Investigation of ligand immobilized nano-composite adsorbent for efficient cerium(III) detection and recovery. *Chem. Eng. J.* **2015**, *265*, 210−218. (e) Awual, M. R.; Hasan, M. M.; Khaleque, M. A. Efficient selenium(IV) detection and removal from water by tailor-made novel conjugate adsorbent. *Sens. Actuators, B* **2015**, *209*, 194−202.

(20) He, Q.; Shi, J. Mesoporous silica nanoparticle based nano drug delivery systems: synthesis, controlled drug release and delivery, pharmacokinetics and biocompatibility. *J. Mat. Chem. C* **2011**, *21*, 5845−5855.

(21) (a) Ismael, M.; Yaita, T. Efficient detection and extraction of cobalt(II) from lithium ion batteries and wastewater by novel composite adsorbent. *Sens. Actuators, B* **2014**, *191*, 9−18. (b) Awual, M. R.; Rahman, I. M. M.; Yaita, T.; Khaleque, M. A.; Ferdows, M. pH dependent Cu(II) and Pd(II) ions detection and removal from aqueous media by an efficient mesoporous adsorbent. *Chem. Eng. J.* **2014**, *236*, 100−109. (c) Shenashen, M. A.; Jyo, A.; Shiwaku, H.; Yaita, T. Preparing of novel fibrous ligand exchange adsorbent for rapid column−mode trace phosphate removal from water. *J. Ind. Eng. Chem.* **2014**, *20*, 2840−2847. (d) Awual, M. R.; Yaita, T. Rapid sensing and recovery of palladium(II) using N,N-bis(salicylidene)1,2-bis(2-aminophenylthio)ethane modified sensor ensemble adsorbent. *Sens. Actuators, B* **2013**, *183*, 332−341. (e) Yaita, T.; Shiwaku, H. Design a novel optical adsorbent for simultaneous ultra-trace cerium(III) detection, sorption and recovery. *Chem. Eng. J.* **2013**, *228*, 327−335.

(22) (a) Awual, M. R.; Kobayashi, T.; Miyazaki, Y.; Motokawa, R.; Shiwaku, H.; Suzuki, S.; Okamoto, Y.; Yaita, T. Selective lanthanide sorption and mechanism using novel hybrid Lewis base (N−methyl−N-phenyl−1,10−phenanthroline−2−carboxamide) ligand modified adsorbent. *J. Hazard. Mater.* **2013**, *252*−*253*, 313−320. (b) Awual, M. R.; Hossain, M. A.; Shenashen, M. A.; Yaita, T.; Suzuki, S.; Jyo, A. Evaluating of arsenic(V) removal from water by weak-base anion exchange adsorbents. *Environ. Sci. Pollut. Res.* **2013**, *20*, 421−430. (c) Khaleque, M. A.; Ferdows, M.; Chowdhury, A. M. S.; Yaita, T. Rapid recognition and recovery of gold(III) with functional ligand immobilized novel mesoporous adsorbent. *Microchem. J.* **2013**, *110*, 591−598. (d) Awual, M. R.; Shenashen, M. A.; Yaita, T.; Shiwaku, H.; Jyo, A. Efficient arsenic(V) removal from water by ligand exchange fibrous adsorbent. *Water Res.* **2012**, *46*, 5541−5550. (e) Jyo, A. Assessing of phosphorus removal by polymeric anion exchangers. *Desalination* **2011**, *281*, 111−117.

(23) (a) Awual, M. R.; Jyo, A. Rapid column-mode removal of arsenate from water by crosslinked poly(allylamine) resin. *Water Res.*

https://doi.org/10.1021/acsomega.2c07377
ACS Omega 2023, 8, 6762−6777

2009, *43*, 1229−1236. (b) Urata, S.; Jyo, A.; Tamada, M.; Katakai, A. Arsenate removal from water by a weak-base anion exchange fibrous adsorbent. *Water Res.* **2008**, *42*, 689−696. (c) Al-tabatabaie, K. F.; Hossain, M. B.; Islam, M. K.; Awual, M. R.; Islam, A. R. M. T.; Hossain, M. A.; Esraz-Ul-Zannat, M.; Islam, A. Taking strides towards decarbonization: The viewpoint of Bangladesh. *Energy Strategy Rev.* **2022**, *44*, 100948. (d) Chowdhury, M. F.; Khandaker, S.; Sarker, F.; Islam, A.; Rahman, M. T.; Awual, M. R. Current treatment technologies and mechanisms for removal of indigo carmine dyes from wastewater: A review. *J. Mol. Liq.* **2020**, *318*, 114061. (e) El-Safty, S. A.; Shenashen, M. A.; Ismael, M.; Khairy, M.; Awual, M. R. Mesoporous aluminosilica sensors for the visual removal and detection of Pd(II) and Cu(II) ions. *Microporous Mesoporous Mater.* **2013**, *166*, 195−205.

(24) (a) Jyo, A.; Ihara, T.; Seko, N.; Tamada, M.; Lim, K. T. Enhanced trace phosphate removal from water by zirconium(IV) loaded fibrous adsorbent. *Water Res.* **2011**, *45*, 4592−4600. (b) Awual, M. R.; Jyo, A.; El-Safty, S. A.; Tamada, M.; Seko, N. A weak-base fibrous anion exchanger effective for rapid phosphate removal from water. *J. Hazard. Mater.* **2011**, *188*, 164−171. (c) El-Safty, S. A.; Jyo, A. Removal of trace arsenic(V) and phosphate from water by a highly selective ligand exchange adsorbent. *J. Environ. Sci.* **2011**, *23*, 1947−1954. (d) El-Safty, S. A.; Awual, M. R.; Shenashen, M. A.; Shahat, A. Simultaneous optical detection and extraction of cobalt(II) from lithium ion batteries using nanocollector monoliths. *Sens. Actuators, B* **2013**, *176*, 1015−1025. (e) El-Safty, S. A.; Shenashen, M. A.; Ismael, M.; Khairy, M.; Awual, M. R. Optical mesosensors for monitoring and removal of ultra-trace concentration of Zn(II) and Cu(II) ions from water. *Analyst* **2012**, *137*, 5278−5290.

(25) (a) El-Safty, S. A.; Shahat, A.; Awual, M. R. Efficient adsorbents of nanoporous aluminosilicate monoliths for organic dyes from aqueous solution. *J. Colloid Interface Sci.* **2011**, *359*, 9−18. (b) El-Safty, S. A.; Shahat, A.; Awual, M. R.; Mekawy, M. Large three-dimensional mesocage pores tailoring silica nanotubes as membrane filters: nanofiltration and permeation flux of proteins. *J. Mater. Chem.* **2011**, *21*, 5593−5603. (c) El-Sayed, W. N.; Elwakeel, K. Z.; Shahat, A.; Awual, M. R. Investigation of novel nanomaterial for the removal of toxic substances from contaminated water. *RSC Adv.* **2019**, *9*, 14167−14175. (d) Hasan, M. M.; Hasan, M. N.; Islam, M. M.; Shenashen, M. A.; Iqbal, J. Biodegradable natural carbohydrate polymeric sustainable adsorbents for efficient toxic dye removal from wastewater. *J. Mol. Liq.* **2020**, *319*, 114356. (e) Hasan, M. N.; Shenashen, M. A.; Hasan, M. M.; Znad, H.; Awual, M. R. Assessing of cesium removal from wastewater using functionalized wood cellulosic adsorbent. *Chemosphere* **2021**, *270*, 128668.

(26) (a) Kobayashi, T.; Shiwaku, H.; Miyazaki, Y.; Motokawa, R.; Suzuki, S.; Okamoto, Y.; Yaita, T. Evaluation of lanthanide sorption and their coordination mechanism by EXAFS measurement using novel hybrid adsorbent. *Chem. Eng. J.* **2013**, *225*, 558−566. (b) Awual, M. R.; Ismael, M.; Yaita, T.; El-Safty, S. A.; Shiwaku, H.; Okamoto, Y.; Suzuki, S. Trace copper(II) ions detection and removal from water using novel ligand modified composite adsorbent. *Chem. Eng. J.* **2013**, *222*, 67−76. (c) Yaita, T.; El-Safty, S. A.; Shiwaku, H.; Okamoto, Y.; Suzuki, S. Investigation of palladium(II) detection and recovery using ligand modified conjugate adsorbent. *Chem. Eng. J.* **2013**, *222*, 172−179. (d) Hasan, M. N.; Salman, M. S.; Islam, A.; Znad, H.; Hasan, M. M. Sustainable composite sensor material for optical cadmium(II) monitoring and capturing from wastewater. *Microchem. J.* **2021**, *161*, 105800. (e) Hasan, M. M.; Shenashen, M. A.; Hasan, M. N.; Znad, H.; Salman, M. S.; Awual, M. R. Natural biodegradable polymeric bioadsorbents for efficient cationic dye encapsulation from wastewater. *J. Mol. Liq.* **2021**, *323*, 114587.

(27) Hudson, S. P.; Padera, R. F.; Langer, R.; Kohane, D. S. The biocompatibility of mesoporous silicates. *Biomaterials* **2008**, *29*, 4045−4055.

(28) (a) Hassan, H. M. A.; Shahat, A.; Azzazy, H. M.; Abd El-aal, R. M.; El-Sayed, W. N.; Elwahed, A.; Awual, M. R. A novel and potential chemical sensor for effective monitoring of Fe(II) ion in corrosion systems of water samples. *Microchem. J.* **2020**, *154*, 104578. (b) Hussain, M. M.; Rahman, M. M.; Asiri, A. M.; Awual, M. R. Non-enzymatic simultaneous detection of L-glutamic acid and uric acid using mesoporous Co3O4 nanospheres. *RSC Adv.* **2016**, *6*, 80511−80521. (c) Islam, A.; Ahmed, M. T.; Mondal, M. A. H.; Awual, M. R.; Monir, M. U.; Islam, K. A snapshot of coal-fired power generation in Bangladesh: A demand−supply outlook. *Nat. Res. Forum* **2021**, *45*, 157−182. (d) Suzuki, S.; Taguchi, T.; Shiwaku, H.; Okamoto, Y.; Yaita, T. Radioactive cesium removal from nuclear wastewater by novel inorganic and conjugate adsorbents. *Chem. Eng. J.* **2014**, *242*, 127−135. (e) Awual, M. R.; Yaita, T.; El-Safty, S. A.; Shiwaku, H.; Suzuki, S.; Okamoto, Y. Copper(II) ions capturing from water using ligand modified a new type mesoporous adsorbent. *Chem. Eng. J.* **2013**, *221*, 322−330.

(29) (a) Hasan, M. M.; Ihara, T.; Yaita, T. Mesoporous silica based novel conjugate adsorbent for efficient selenium(IV) detection and removal from water. *Micropoous. Mesoporous Mater.* **2014**, *197*, 331−338. (b) Awual, M. R.; Yaita, T.; Taguchi, T.; Shiwaku, H.; Suzuki, S.; Okamoto, Y. Selective cesium removal from radioactive liquid waste by crown ether immobilized new class conjugate adsorbent. *J. Hazard. Mater.* **2014**, *278*, 227−235. (c) Islam, A.; Hossain, M. B.; Mondal, M. A. H.; Ahmed, M. T.; Hossain, M. A.; Monir, M. U.; Khan, M. F. H.; Islam, K.; Khandaker, S.; Choudhury, T. R.; Awual, M. R. Energy challenges for a clean environment: Bangladesh's experience. *Energy Rep.* **2021**, *7*, 3373−3389. (d) Islam, A.; Roy, S.; Khan, M. A.; Mondal, P.; Teo, S. H.; Taufiq-Yap, Y. H.; Ahmed, M. T.; Choudhury, T. R.; Alsultan, G. A.; Khandaker, S. Improving valuable metal ions capturing from spent Li-ion batteries with novel materials and approaches. *J. Mol. Liq.* **2021**, *338*, 116703. (e) Islam, A.; Hwa Teo, S.; Awual, M. R.; Taufiq-Yap, Y. H. Ultrathin assembles of porous array for enhanced H_2 evolution. *Sci. Rep.* **2020**, *10*, 2324.

(30) (a) Hasan, M. M. A novel fine-tuning mesoporous adsorbent for simultaneous lead(II) detection and removal from wastewater. *Sens. Actuators, B* **2014**, *202*, 395−403. (b) Awual, M. R.; Hasan, M. M.; Shahat, A. Functionalized novel mesoporous adsorbent for selective lead(II) ions monitoring and removal from wastewater. *Sens. Actuators, B* **2014**, *203*, 854−863. (c) Islam, A.; Ahmed, T.; Awual, M. R.; Rahman, A.; Sultana, M.; Aziz, A. A.; Monir, M. U.; Teo, S. H.; Hasan, M. Advances in sustainable approaches to recover metals from e-waste-A review. *J. Clean. Prod.* **2020**, *244*, 118815. (d) Islam, A.; Teo, S. H.; Awual, M. R.; Taufiq-Yap, Y. H. Assessment of clean H_2 energy production from water using novel silicon photocatalyst. *J. Clean. Prod.* **2020**, *244*, 118805. (e) Islam, M. A.; Angove, M. J.; Morton, D. W.; Pramanik, B. K.; Awual, M. R. A mechanistic approach of chromium(VI) adsorption onto manganese oxides and boehmite. *J. Environ. Chem. Eng.* **2020**, *8*, 103515.

(31) (a) Hasan, M. M.; Znad, H. Organic-inorganic based nano-conjugate adsorbent for selective palladium(II) detection, separation and recovery. *Chem. Eng. J.* **2015**, *259*, 611−619. (b) Awual, M. R.; Hasan, M. M.; Naushad, M.; Shiwaku, H.; Yaita, T. Preparation of new class composite adsorbent for enhanced palladium(II) detection and recovery. *Sens. Actuators, B* **2015**, *209*, 790−797. (c) Islam, M. A.; Awual, M. R.; Angove, M. J. A review on nickel(II) adsorption in single and binary component systems and future path. *J. Environ. Chem. Eng.* **2019**, *7*, 103305. (d) Islam, A.; Teo, S. H.; Awual, M. R.; Taufiq-Yap, Y. H. Improving the hydrogen production from water over MgO promoted Ni-Si/CNTs photocatalyst. *J. Clean. Prod.* **2019**, *238*, 117887. (e) Kamel, R. M.; Shahat, A.; Hegazy, W. H.; Khodier, E. M.; Awual, M. R. Efficient toxic nitrite monitoring and removal from aqueous media with ligand based conjugate materials. *J. Mol. Liq.* **2019**, *285*, 20−26.

(32) (a) Khaleque, M. A.; Ratna, Y.; Znad, H. Simultaneous ultra-trace palladium(II) detection and recovery from wastewater using new class meso-adsorbent. *J. Ind. Eng. Chem.* **2015**, *21*, 405−413. (b) Karim, M. R.; Aijaz, M. O.; Alharth, N. H.; Alharbi, H. F.; Al-Mubaddel, F. S.; Awual, M. R. Composite nanofibers membranes of poly(vinyl alcohol)/chitosan for selective lead(II) and cadmium(II) ions removal from wastewater. *Ecotoxicol. Environ. Saf.* **2019**, *169*, 479−486. (c) Khandaker, S.; Chowdhury, M. F.; Islam, A.; Kuba, T. Efficient cesium encapsulation from contaminated water by cellulosic

https://doi.org/10.1021/acsomega.2c07377
ACS Omega 2023, 8, 6762−6777

biomass based activated wood charcoal. *Chemosphere* **2021**, *262*, 127801. (d) Khandaker, S.; Toyohara, Y.; Saha, G. C.; Kuba, T.; Awual, M. R. Development of synthetic zeolites from bio-slag for cesium adsorption: kinetic, isotherm and thermodynamic studies. *J. Water Process Eng.* **2020**, *33*, 101055. (e) Kubra, K. T.; Salman, M. S.; Hasan, M. N. Enhanced toxic dye removal from wastewater using biodegradable polymeric natural adsorbent. *J. Mol. Liq.* **2021**, *328*, 115468.

(33) Ioannou-Ttofa, L.; Raj, S.; Prakash, H.; Fatta-Kassinos, D. Solar photo-Fenton oxidation for the removal of ampicillin, total cultivable and resistant *E. coli* and ecotoxicity from secondary-treated wastewater effluents. *Chem. Eng. J.* **2019**, *355*, 91−102.

(34) Pulicharla, R.; Hegde, K.; Brar, S. K.; Surampalli, R. Y. Tetracyclines metal complexation: Significance and fate of mutual existence in the environment. *Environ. Pollut., Ser. B.* **2017**, *221*, 1−14.

(35) Brühwiler, D. Postsynthetic functionalization of mesoporous silica. *Nanoscale* **2010**, *2*, 887−892.

(36) Wang, B.; Lv, X.-L.; Feng, D.; Xie, L.-H.; Zhang, J.; Li, M.; Xie, Y.; Li, J.-R.; Zhou, H.-C. Highly stable Zr (IV)-based metal−organic frameworks for the detection and removal of antibiotics and organic explosives in water. *J. Am.Chem. Soc.* **2016**, *138*, 6204−6216.

(37) Chung, T.-H.; Wu, S.-H.; Yao, M.; Lu, C.-W.; Lin, Y.-S.; Hung, Y.; Mou, C.-Y.; Chen, Y.-C.; Huang, D.-M. The effect of surface charge on the uptake and biological function of mesoporous silica nanoparticles in 3T3-L1 cells and human mesenchymal stem cells. *Biomaterials* **2007**, *28*, 2959−2966.

(38) (a) Mazrouaa, A. M.; Mansour, N. A.; Abed, M. Y.; Youssif, M. A.; Shenashen, M. A.; Awual, M. R. Nano-composite multi-wall carbon nanotubes using poly(pphenylene terephthalamide) for enhanced electric conductivity. *J. Environ. Chem. Eng.* **2019**, *7*, 103002. (b) Mohamed, S. K.; Hassan, H. M. A.; Shahat, A.; Awual, M. R.; Kamel, R. M. A ligand-based conjugate solid sensor for colorimetric ultra-trace gold(III) detection in urban mining waste. *Colloids Surf. A* **2019**, *581*, 123842. (c) Naushad, M.; Alqadami, A. A.; Al-Kehtani, A. A.; Ahamad, T.; Tatarchuk, T. Adsorption of textile dye using para-aminobenzoic acid modified activated carbon: Kinetic and equilibrium studies. *J. Mol. Liq.* **2019**, *296*, 112075. (d) Naushad, M.; Khan, M. R.; ALOthman, Z. A.; Al-Muhtaseb, A. H.; Alqadami, A. A. Water purification using cost effective material prepared from agricultural waste: Kinetics, isotherms and thermodynamic studies. *Clean-Soil Air Water* **2016**, *44*, 1036−1045. (e) Naushad, M.; AlOthman, Z. A.; Ahamad, T. Adsorption of Rose Bengal dye from aqueous solution by amberlite IRA-938 resin: Kinetics, isotherms and thermodynamic studies. *Desalination Water Treat.* **2016**, *57*, 13527−13533.

(39) (a) Kubra, K. T.; Salman, M. S.; Znad, H.; Hasan, M. N. Efficient encapsulation of toxic dye from wastewater using biodegradable polymeric adsorbent. *J. Mol. Liq.* **2021**, *329*, 115541. (b) Kubra, K. T.; Salman, M. S.; Hasan, M. N.; Islam, A.; Teo, S. H.; Hasan, M. M.; Sheikh, M. C.; Awual, M. R. Sustainable detection and capturing of cerium(III) using ligand embedded solid-state conjugate adsorbent. *J. Mol. Liq.* **2021**, *338*, 116667. (c) Naushad, M.; Khan, M. R.; ALOthman, Z. A. Bromate removal from water samples using strongly basic anion exchange resin Amberlite IRA-400: Kinetics, isotherms and thermodynamic studies. *Desalination Water Treat.* **2016**, *57*, 5781−5788. (d) Naushad, M.; AlOthman, Z. A.; Alam, M. M.; Eldesoky, G. E.; Islam, M. Synthesis of sodium dodecyl sulfate-supported nanocomposite cation exchanger: removal and recovery of Cu^{2+} from synthetic, pharmaceutical and alloy samples. *J. Iran. Chem. Soc.* **2015**, *12*, 1677−1686. (e) Naushad, M.; ALOthman, Z. A.; Awual, M. R.; Alam, M. M.; Eldesoky, G. E. Adsorption kinetics, isotherms and thermodynamic studies for the adsorption of Pb^{2+} and Hg^{2+} metal ions from aqueous medium using Ti(IV) iodovanadate cation exchanger. *Ionics* **2015**, *21*, 2237−2245.

(40) (a) Rahman, M. M.; Hussain, M. M.; Arshad, M. N.; Asiri, A. M. Arsenic sensor development based on modification with (E)-N′-(2-nitrobenzylidine)- benzenesulfonohydrazide: a real sample analysis. *New J. Chem.* **2019**, *43*, 9066−9075. (b) Rahman, M. M.; Alam, M. M.; Asiri, A. M.; Awual, M. R. Fabrication of 4-aminophenol sensor based on hydrothermally prepared ZnO/Yb2O3 nanosheets. *New J. Chem.* **2017**, *41*, 9159−9169. (c) Roy, B. C.; Awual, M. R.; Goto, M. Effect of inorganic salts on ternary equilibrium data of propionic acid-water-solvents systems. *J. App. Sci.* **2007**, *7*, 1053−1060. (d) Salman, M. S.; Znad, H.; Hasan, M. N.; Hasan, M. M. Optimization of innovative composite sensor for Pb(II) detection and capturing from water samples. *Microchem. J.* **2021**, *160*, 105765. (e) Shahat, A.; Awual, M. R.; Kubra, K. T.; Salman, M. S.; Hasan, M. N.; Hasan, M. M. Novel solid-state sensor material for efficient cadmium(II) detection and capturing from wastewater. *Microchem. J.* **2021**, *164*, 105967.

(41) (a) Shahat, A.; Khaleque, M. A.; Alam, M. Z.; Naushad, M.; Chowdhury, A. M. S. Large-pore diameter nano-adsorbent and its application for rapid lead(II) detection and removal from aqueous media. *Chem. Eng. J.* **2015**, *273*, 286−295. (b) Shahat, A.; Naushad, M. Functional ligand anchored nanomaterial based facial adsorbent for cobalt(II) detection and removal from water samples. *Chem. Eng. J.* **2015**, *271*, 155−163. (c) Sharavanan, V. J.; Sivaramakrishnan, M.; Sivarajasekar, N.; Senthilrani, N.; Kothandan, R.; Dhakal, N.; Sivamani, S.; Show, P. L.; Naushad, M. Pollutants inducing epigenetic changes and diseases. *Environ. Chem. Lett.* **2020**, *18*, 325−343. (d) Sheikh, T. A.; Arshad, M. N.; Rahman, M. M.; Asiri, A. M.; Marwani, H. M.; Bawazir, W. A. Trace electrochemical detection of Ni^{2+} ions with bidentate *N*, *N*′-(ethane-1,2-diyl)bis(3,4-dimethoxybenzenesulfonamide) [EDBDMBS] as a chelating agent. *Inorgan. Chim. Acta* **2017**, *464*, 157−166. (e) Shahat, A.; Hassan, H. M. A.; Azzazy, H. M. E.; Hosni, M.; Awual, M. R. Novel nano-conjugate materials for effective arsenic(V) and phosphate capturing in aqueous media. *Chem. Eng. J.* **2018**, *331*, 54−63.

(42) (a) Roy, B. C.; Goto, M. Liquid-liquid equilibrium data for the ternary systems of propionic acid-water-solvents. *J. Appl. Sci.* **2006**, *6*, 411−415. (b) Salman, M. S.; Hasan, M. N.; Kubra, K. T.; Hasan, M. M. Optical detection and recovery of Yb(III) from waste sample using novel sensor ensemble nanomaterials. *Microchem. J.* **2021**, *162*, 105868. (c) Shahat, A.; Mohamed, M. H.; Mohamed, S. K. Novel and potential chemical sensors for Au(III) ion detection and recovery in electric waste samples. *Microchem. J.* **2020**, *158*, 105312. (d) Shahat, A.; Hassan, H. M. A.; El-Shahat, M. F.; El-Shahawy, O. A ligand-anchored optical composite material for efficient vanadium(II) adsorption and detection in wastewater. *New J. Chem.* **2019**, *43*, 10324−10335. (e) Sheikh, T. A.; Rahman, M. M.; Asiri, A. M.; Marwani, H. M.; Awual, M. R. 4-Hexylresorcinol sensor development based on wet-chemically prepared Co3O4@Er2O3 nanorods: A practical approach. *J. Ind. Eng. Chem.* **2018**, *66*, 446−455.

(43) Shahat, A.; Elamin, N. Y.; Abd El-Fattah, W. Spectrophotometric and Fluorometric Methods for the Determination of Fe (III) Ions in Water and Pharmaceutical Samples. *J. ACS omega* **2022**, *7*, 1288−1298.

(44) Gamil, A. A.; Al-Hazmi; Mohamed, A.; El-Bindary; Mohamed, G.; El-Desouky; El-Bindary, A. A. Efcient adsorptive removal of industrial dye from aqueous solution by synthesized zeolitic imidazolate framework-8 loaded date seed activated carbon and statistical physics modeling. *Desalin. Water Treat.* **2022**, *258*, 85−103.

(45) Abou-Melha, K. S.; Al-Hazmi, G. A.; Habeebullah, T. M.; Althagafi, I.; Othman, A.; El-Metwaly, N. M.; Shaaban, F.; Shahat, A. Functionalized silica nanotubes with azo-chromophore for enhanced Pd^{2+} and Co^{2+} ions monitoring in E-wastes. *J. Mol. Liq.* **2021**, *329*, 115585.

(46) Altalhi, T. A.; Ibrahim, M. M.; Mersal, G. A.; Alsawat, M.; Mahmoud, M.; Kumeria, T.; Shahat, A.; El-Bindary, M. J. A. C. A. Mesopores silica nanotubes-based sensors for the highly selective and rapid detection of Fe^{2+} ions in wastewater, boiler system units and biological samples. 2021, *1180*, 338860.

(47) El-Safty, S.; Shahat, A.; Ogawa, K.; Hanaoka, T. Highly ordered, thermally/hydrothermally stable cubic Ia3d aluminosilica monoliths with low silica in frameworks. *Microporous Mesoporous Mater.* **2011**, *138*, 51−62.

(48) El-Desouky, M. G.; Hassan, N.; Shahat, A.; El-Didamony, A.; El-Bindary, A. A. Synthesis and characterization of porous magnetite

https://doi.org/10.1021/acsomega.2c07377
ACS Omega 2023, 8, 6762−6777

nanosphere iron oxide as a novel adsorbent of anionic dyes removal from aqueous solution. *Biointerface Res. Appl. Chem.* **2021**, *11*, 13377−13401.
(49) (a) Rahman, M. M.; Alamry, K. A.; Mekky, A. E. M. Efficient Hg(II) ionic probe development based on one-step synthesized diethyl thieno[2,3-b]thiophene-2,5-dicarboxylate (DETTDC2) onto glassy carbon electrode. *Microchem. J.* **2020**, *152*, 104291. (b) Rahman, M. M.; Sheikh, T. A.; Asiri, A. M.; Awual, M. R. Development of 3-methoxyanaline sensor probe based on thin Ag2O@La2O3 nano-sheets for environmental safety. *New J. Chem.* **2019**, *43*, 4620−4632. (c) Shahat, A.; Hassan, H. M. A.; El-Shahat, M. F.; El Shahawy, O. Visual nickel(II) ions treatment in petroleum samples using a mesoporous composite adsorbent. *Chem. Eng. J.* **2018**, *334*, 957−967. (d) Shahat, A.; Hassan, H. M. A.; Azzazy, H. M. E.; El-Sharkawy, E. A.; Abdou, H. M. Novel hierarchical composite adsorbent for selective lead(II) ions capturing from wastewater samples. *Chem. Eng. J.* **2018**, *332*, 377−386. (e) Teo, S. H.; Islam, A.; Chan, E. S.; Choong, S. Y. T.; Alharthi, N. H.; Taufiq-Yap, Y. H. Efficient biodiesel production from Jatropha curcus using $CaSO_4/Fe_2O_3$-SiO_2 core-shell magnetic nanoparticles. *J. Cleaner Prod.* **2019**, *208*, 816−826.
(50) (a) Rahman, M. M.; Asiri, A. M. Preparation and evaluation of composite hybrid nanomaterials for rare-earth elements separation and recovery. *Sep. Purif. Technol.* **2020**, *253*, 117515. (b) Rahman, M. M.; Wahid, A.; Asiri, A. M.; Karim, M. R. One-step facile synthesis of SnO2@Nd2O3 nanocomposites for selective amidol detection in aqueous phase. *New J. Chem.* **2020**, *44*, 4952−4959. (c) Teo, S. H.; Islam, A.; Taufiq-Yap, Y. H.; Awual, M. R. Introducing the novel composite photocatalysts to boost the performance of hydrogen (H_2) production. *J. Cleaner Prod.* **2021**, *313*, 127909. (d) Yeamin, M. B.; Islam, M. M.; Chowdhury, A. N.; Awual, M. R. Efficient encapsulation of toxic dyes from wastewater using several biodegradable natural polymers and their composites. *J. Cleaner Prod.* **2021**, *291*, 125920. (e) Znad, H.; Abbas, K.; Hena, S.; Awual, M. R. Synthesis a novel multilamellar mesoporous TiO2/ZSM-5 for photo-catalytic degradation of methyl orange dye in aqueous media. *J. Environ. Chem. Eng.* **2018**, *6*, 218−227.
(51) Pan, J.; Bai, X.; Li, Y.; Yang, B.; Yang, P.; Yu, F.; Ma, J. HKUST-1 derived carbon adsorbents for tetracycline removal with excellent adsorption performance. *Environ. Res.* **2022**, *205*, 112425.
(52) (a) Kubra, K. T.; Salman, M. S.; Hasan, M. N.; Islam, A.; Hasan, M. M.; Awual, M. R. Utilizing an alternative composite material for effective copper(II) ion capturing from wastewater. *J. Mol. Liq.* **2021**, *336*, 116325. (b) Znad, H.; Al-Mohammedawi, H. Integrated pre-treatment stage of biosorbent-sonication for mixed brewery and restaurant effluents to enhance the photo-fermentative hydrogen production. *Biomass Bioenergy* **2021**, *144*, 105899. (c) Islam, A.; Teo, S. H.; Taufiq-Yap, Y. H.; Vo, D. V. N.; Awual, M. R. Towards the robust hydrogen (H_2) fuel production with niobium complexes-A review. *J. Clean. Prod.* **2021**, *318*, 128439. (d) Islam, A.; Teo, S. H.; Taufiq-Yap, Y. H.; Ng, C. H.; Vo, D. V. N.; Ibrahim, M. L.; Hasan, M. M.; Khan, M. A. R.; Nur, A. S. M.; Awual, M. R. Step towards the sustainable toxic dyes and heavy metals removal and recycling from aqueous solution- A comprehensive review. *Resour. Conserv. Recy.* **2021**, *175*, 105849. (e) Miah, M. R.; Yang, M.; Hossain, M. M.; Khandaker, S.; Awual, M. R. Textile-based flexible and printable sensors for next generation uses and their contemporary challenges: A critical review. *Sens. Actuators, A* **2022**, *344*, 113696.
(53) (a) Khandaker, S.; Bashar, M. M.; Islam, A.; Hossain, M. T.; Teo, S. H.; Awual, M. R. Sustainable energy generation from textile biowaste and its challenges: A comprehensive review. *Renew. Sust. Energ. Rev.* **2022**, *157*, 112051. (b) Znad, H.; Martini, S. The utilization of algae and seaweed biomass for bioremediation of heavy metal-contaminated wastewater. *Molecules* **2022**, *27*, 1275. (c) Kabir, M. M.; Akter, M. M.; Khandaker, S.; Gilroyed, B. H.; Alam, M. D.; Hakim, M. Highly effective agro-waste based functional green adsorbents for toxic chromium(VI) ion removal from wastewater. *J. Mol. Liq.* **2022**, *347*, 118327. (d) Teo, S. H.; Ng, C. H.; Islam, A.; Abdulkareem-Alsultan, G.; Joseph, C. G.; Janaun, J.; Taufiq-Yap, Y. H.; Khandaker, S.; Islam, G. J.; Znad, H. Sustainable toxic dyes removal with advanced materials for clean water production: A comprehensive review. *J. Cleaner Prod.* **2022**, *332*, 130039. (e) Rajendran, S.; Hoang, T. K. A.; Trudeau, M. L.; Jalil, A. A.; Naushad, M.; Awual, M. R. Generation of novel n-p-n (CeO_2-PPy-ZnO) heterojunction for photocatalytic degradation of micro-organic pollutants. *Environ. Pollut.* **2022**, *292*, 118375.
(54) Zhao, Y.; Geng, J.; Wang, X.; Gu, X.; Gao, S. Tetracycline adsorption on kaolinite: pH, metal cations and humic acid effects. *J. Ecotoxicology* **2011**, *20*, 1141−1147.
(55) El-Desouky, M.; El-Bindary, A. Magnetic metal-organic framework (Fe3O4@ ZIF-8) nanocomposites for adsorption of anionic dyes from wastewater. *Inorganic Nano-Metal Chemistry* **2021**, 1−15.
(56) (a) Islam, A.; Roy, S.; Teo, S. H.; Khandaker, S.; Taufiq-Yap, Y. H.; Aziz, A. A.; Monir, M. U.; Rashid, U.; Vo, D. V. N.; Ibrahim, M. L.; Znad, H.; Awual, M. R. Functional novel ligand based palladium(II) separation and recovery from e-waste using solvent-ligand approach. *Colloids Surf., A* **2022**, *632*, 127767. (b) Khandaker, S.; Das, S.; Hossain, M. T.; Islam, A.; Miah, M. R. Sustainable approach for wastewater treatment using microbial fuel cells and green energy generation- A comprehensive review. *J. Mol. Liq.* **2021**, *344*, 117795. (c) Khandaker, S.; Hossain, M. T.; Saha, P. K.; Rayhan, U.; Islam, A.; Choudhury, T. R.; Awual, M. R. Functionalized layered double hydroxides composite bio-adsorbent for efficient copper(II) ion encapsulation from wastewater. *J. Environ. Manage.* **2021**, *300*, 113782. (d) Islam, A.; Swaraz, A. M.; Teo, S. H.; Taufiq-Yap, Y. H.; Vo, D. V. N.; Ibrahim, M. L.; Abdulkreem-Alsultan, G.; Rashid, U.; Awual, M. R. Advances in physiochemical and biotechnological approaches for sustainable metal recovery from e-waste: A critical review. *J. Cleaner Prod.* **2021**, *323*, 129015. (e) Rahman, M. S.; Ahmed, A. S. S.; Rahman, M. M.; Babu, S. M. O. F.; Sultana, S.; Sarker, S. I.; Rahman, M. M.; Rahman, M. Temporal assessment of heavy metal concentration and surface water quality representing the public health evaluation from the Meghna River estuary, Bangladesh. *Appl. Water Sci.* **2021**, *11*, 121.
(57) Al-Hazmi, G. H.; Adam, A. M. A.; El-Desouky, M. G.; El-Bindary, A. A.; Alsuhaibani, A. M.; Refat, M. S. Efficient adsorption of Rhodamine B using a composite of Fe3O4@ zif-8: Synthesis, characterization, modeling analysis, statistical physics and mechanism of interaction. *Bull. Chem. Soc. Ethiop.* **2023**, *37*, 211−229.
(58) Langmuir, I. The constitution and fundamental properties of solids and liquids. Part I. Solids. *Am. Chem. Soc* **1916**, *38*, 2221−2295.
(59) Freundlich, H. M. F. Over the adsorption in solution. *J. Phys. Chem.* **1906**, *57*, 385−471.
(60) Dubinin, M. The equation of the characteristic curve of activated charcoal. *Proc. Acad. Sci. USSR Phys. Chem. Sect.* **1947**, *55*, 327−329.
(61) Tempkin, M. I.; Pyzhev, V. J. A. P. C. Kinetics of ammonia synthesis on promoted iron catalyst. *Acta Phys. Chim. USSR* **1940**, *12*, 327−356.
(62) Lagergren, S. K. About the theory of so-called adsorption of soluble substances. *Sven. Vetenskapsakad. Handingarl* **1898**, *24*, 1−39.
(63) Ho, Y.-S.; McKay, G. Pseudo-second order model for sorption processes. *Process Biochem.* **1999**, *34*, 451−465.
(64) Weber, W. J., Jr.; Morris, J. C. Kinetics of adsorption on carbon from solution. *J. Sanit. Eng. Div.* **1963**, *89*, 31−59.
(65) Hassan, N.; Shahat, A.; El-Didamony, A.; El-Desouky, M. G.; El-Bindary, A. A. Synthesis and characterization of ZnO nanoparticles via zeolitic imidazolate framework-8 and its application for removal of dyes. *J. Mol. Struct.* **2020**, *1210*, 128029.
(66) Zeldowitsch, J. The catalytic oxidation of carbon monoxide on manganese dioxide. *Acta Physicochim. URSS* **1934**, *1*, 364−449.
(67) (a) El-Desouky, M. G.; Shahat, A.; El-Bindary, A. A.; El-Bindary, M. A. Description, Kinetic and Equilibrium Studies of the Adsorption of Carbon Dioxide in Mesoporous Iron Oxide Nano-spheres. *Biointerface Res. Appl. Chem.* **2021**, *12*, 3034−3054. (b) Jyo, A.; Tamada, M.; Katakai, A. Zirconium(IV) loaded bifunctional fiber containing both phosphonate and sulfonate as arsenate adsorbent. *J.*

https://doi.org/10.1021/acsomega.2c07377
ACS Omega 2023, 8, 6762−6777

Ion Exchang. **2007**, *18*, 422−427. (c) Al-Hazmi, G. H.; Refat, M. S.; Alshammari, K. F.; Kubra, K. T.; Shahat, A. Efficient toxic doxorubicin hydrochloride removal from aqueous solutions using facial alumina nanorods. *J. Mol. Struct.* **2023**, *1272*, 134187.

(68) (a) Islam, A.; Teo, S. H.; Ng, C. H.; Taufiq-Yap, Y. H.; Choong, S. Y. T.; Awual, M. R. Progress in recent sustainable materials for greenhouse gas (NO_x and SO_x) emission mitigation. *Prog. Mater. Sci.* **2023**, *132*, 101033. (b) Hasan, M. N.; Salman, M. S.; Hasan, M. M.; Kubra, K. T.; Sheikh, M. C.; Rehan, A. I.; Rasee, A. I.; Waliullah, R. M.; Hossain, M. S.; Islam, A.; Khandaker, S.; Alsukaibi, A. K. D.; Alshammari, H. M. Assessing sustainable Lutetium(III) ions adsorption and recovery using novel composite hybrid nanomaterials. *J. Mol. Struct.* **2023**, 134795. (c) Hossain, M. T.; Khandaker, S.; Bashar, M. M.; Islam, A.; Ahmed, M.; Akter, R.; Alsukaibi, A. K. D.; Hasan, M. M.; Alshammari, H. M.; Kuba, T. Simultaneous toxic Cd(II) and Pb(II) encapsulation from contaminated water using Mg/Al-LDH composite materials. *J. Mol. Liq.* **2022**, *368*, 120810. (d) Miah, M. R.; Yang, M.; Khandaker, S.; Bashar, M. M.; Alsukaibi, A. K. D.; Hassan, H. M. A.; Znad, H.; Awual, M. R. Polypyrrole-based sensors for volatile organic compounds (VOCs) sensing and capturing: A comprehensive review. *Sensor. Actuat. A: Phy.* **2022**, *347*, 113933. (e) Jahan, A.; Alam, M. A.; Akhtar, S. Volumetric and acoustic properties for binary mixtures of N,N-Dimethylformamide with 2-butanol and 2-pentanol at temperatures between 298.15 K and 318.15 K. *Am. J. Chem.* **2019**, *9*, 1−12.

https://doi.org/10.1021/acsomega.2c07377
ACS Omega 2023, 8, 6762−6777